JGR Solid Earth

RESEARCH ARTICLE
10.1029/2020JB019743

Geological and Thermal Control of the Hydrothermal System in Northern Yellowstone Lake: Inferences From High-Resolution Magnetic Surveys

Claire Bouligand[1], Maurice A. Tivey[2], Carol A. Finn[3], Lisa A. Morgan[3], W. C. Pat Shanks III[3], and Robert A. Sohn[2]

[1]Université Grenoble Alpes, Université Savoie Mont Blanc, CNRS, IRD, IFSTTAR, ISTerre, Grenoble, France, [2]Woods Hole Oceanographic Institution, Woods Hole, MA, USA, [3]U.S. Geological Survey, Denver, CO, USA

Key Points:
- Multiscale magnetic surveys of northern Yellowstone lake display a striking correlation between magnetic lows and hydrothermal activity
- Forward and inverse modeling is used to investigate lake floor magnetization in relation to geology, heat flow, and hydrothermal alteration
- A detailed survey over a sublacustrine vapor-dominated vent shows reduced magnetization restricted to the vent periphery

Supporting Information:
- Supporting Information S1

Correspondence to:
C. Bouligand,
claire.bouligand@univ-grenoble-alpes.fr

Citation:
Bouligand, C., Tivey, M. A., Finn, C. A., Morgan, L. A., Shanks, W. C. P., III, & Sohn, R. A. (2020). Geological and thermal control of the hydrothermal system in northern Yellowstone Lake: Inferences from high-resolution magnetic surveys. *Journal of Geophysical Research: Solid Earth*, *125*, e2020JB019743. https://doi.org/10.1029/2020JB019743

Received 10 MAR 2020
Accepted 22 JUL 2020
Accepted article online 27 JUL 2020

Abstract A multiscale magnetic survey of the northern basin of Yellowstone Lake was undertaken in 2016 as part of the Hydrothermal Dynamics of Yellowstone Lake Project (HD-YLAKE)—a broad research effort to characterize the cause-and-effect relationships between geologic and environmental processes and hydrothermal activity on the lake floor. The magnetic survey includes lake surface, regional aeromagnetic, and near-bottom autonomous underwater vehicle (AUV) data. The study reveals a strong contrast between the northeastern lake basin, characterized by a regional magnetic low punctuated by stronger local magnetic lows, many of which host hydrothermal vent activity, and the northwestern lake basin with higher-amplitude magnetic anomalies and no obvious hydrothermal activity or punctuated magnetic lows. The boundary between these two regions is marked by a steep gradient in heat flow and magnetic values, likely reflecting a significant structure within the currently active ~20-km-long Eagle Bay-Lake Hotel fault zone that may be related to the ~2.08-Ma Huckleberry Ridge caldera rim. Modeling suggests that the broad northeastern magnetic low reflects both a shallower Curie isotherm and widespread hydrothermal activity that has demagnetized the rock. Along the western lake shoreline are sinuous-shaped, high-amplitude magnetic anomaly highs, interpreted as lava flow fronts of upper units of the West Thumb rhyolite. The AUV magnetic survey shows decreased magnetization at the periphery of the active Deep Hole hydrothermal vent. We postulate that lower magnetization in the outer zone results from enhanced hydrothermal alteration of rhyolite by hydrothermal condensates while the vapor-dominated center of the vent is less altered.

Plain Language Summary Despite many previous investigations, uncertainties remain about the circulation of hot fluids and gas below the floor of Yellowstone Lake. In this study, we use measurements of the strength of the magnetic field at different heights above the lake floor (via plane, helicopter, boat, and autonomous submersible) to study the rock magnetization, which is a physical property caused by the presence of magnetic minerals. Magnetization varies with rock type, temperature, and hydrothermal alteration of the rock. Our results show that rocks beneath the northeastern part of the lake are less magnetized because of higher temperatures at depth and intense and widespread circulation of hot fluids in the lake floor that destroys magnetic minerals in the rock. In contrast, stronger magnetization beneath the northwestern lake basin suggests that volcanic rocks are unaltered because of lower temperatures and the absence of similar hot fluid circulation at depth. Our measurements allow us to observe structures in the subsurface that might be paths or barriers to fluids. The submersible measurements acquired near the lake floor show decreased rock magnetization at the periphery of a hot gas venting area, where mixing with lower-temperature waters allows the gas to condense and efficiently alter the rock.

1. Introduction

Yellowstone National Park (YNP) is well known for its geothermal features, including the iconic Old Faithful Geyser, the travertine terraces at Mammoth Hot Springs, and thousands of other vents, geysers, fumaroles, and thermal pools. Less well known are the hydrothermal features associated with Yellowstone Lake (Morgan et al., 2003), which at 341 km^2 is among North America's largest high-altitude freshwater lakes (Figure 1). Yellowstone Lake is the third most significant thermal basin in YNP after Upper Geyser and Lower Geyser Basins, based on the chloride flux (Balistrieri et al., 2007; Fournier

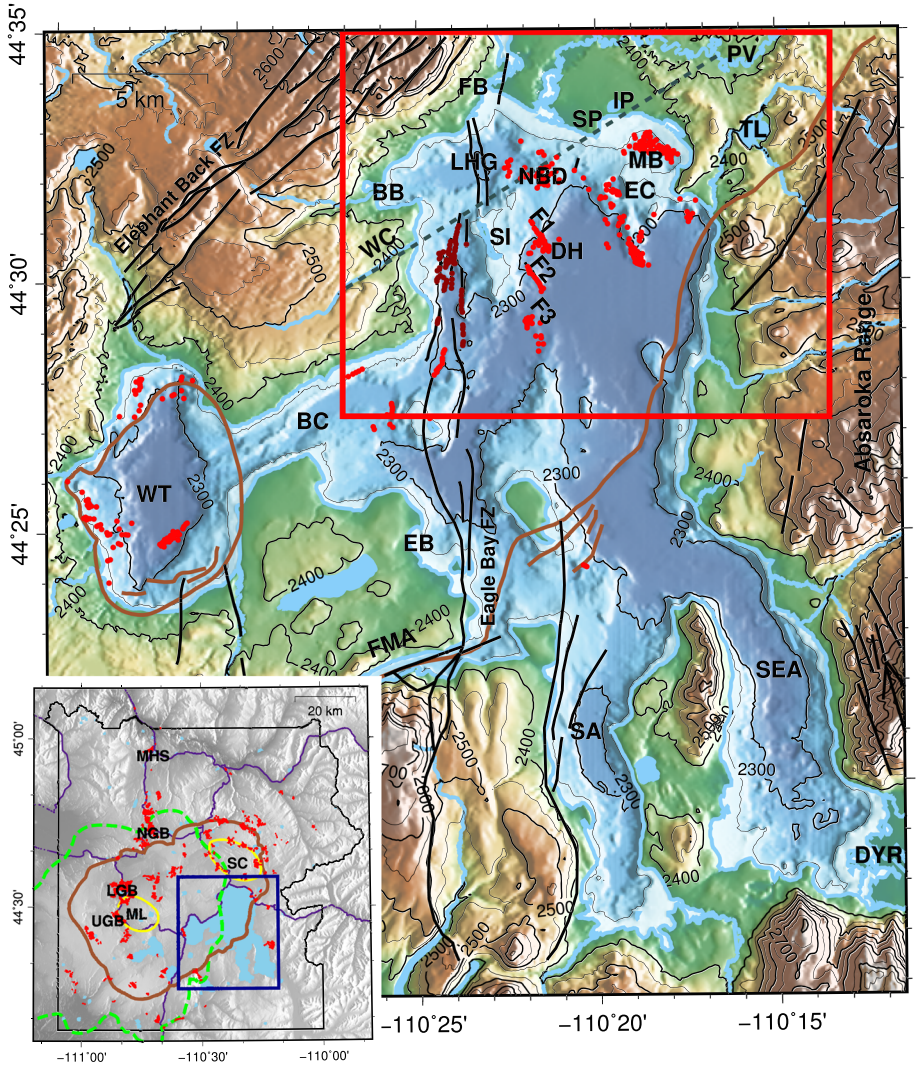

Figure 1. Topographic and bathymetric map of Yellowstone Lake and vicinity showing the distribution of faults (black), the 0.63-Ma Yellowstone caldera rim (brown), and hydrothermal vents (red dots), Weasel Creek lineament (dashed gray line) from Morgan et al. (2007). Dark red dots are features along fissures that were initially labeled as hydrothermal vents (Morgan et al., 2003, 2007), but we discarded this interpretation in this study (see section 5). The outline of Figures 2, 3a, 4, and 6b is shown by the red rectangle. Also shown are the locations of Bridge Bay (BB), Breeze Channel (BC), the "Deep Hole" site (DH), the delta of Yellowstone River (DYR), Eagle Bay (EB), Elliott's crater (EC), Fishing Bridge (FB), Flat Mountain Arm (FMA), Indian Pond (IP), the Lake Hotel graben (LHG), Mary Bay (MB), the Northern Basin hydrothermal dome (NBD), South Arm (SA), Southeast Arm (SEA), Stevenson Island (SI), Storm Point (SP), Turbid Lake (TL), Weasel Creek (WC), and West Thumb (WT). F1, F2, and F3 refer to alignments of hydrothermal vents discussed in the text. The inset shows a shaded topographic map with on-land thermal areas (red), the 0.63-Ma Yellowstone (thick brown outline), and the 2.08-Ma Huckleberry Ridge (thick green dashed outline) caldera rims, and the resurgent Mallard Lake (ML) and (SC) Sour Creek domes (yellow outline) from Christiansen et al. (2007). Also shown are the Yellowstone National Park boundary (thin black line), the main roads (thin dark purple lines), the outline of the main map (blue rectangle), and the locations of Mammoth Hot Springs (MHS), Norris (NGB), Lower (LGB), and Upper (UGB) Geyser Basins. Note that the Huckleberry Ridge caldera rim represented in the inset is approximate and likely crosses the lake more to the east, along the Eagle Bay fault zone (Morgan et al., 2007, 2009).

et al., 1975; Friedman & Norton, 2007; Norton & Friedman, 1985; Shanks et al., 2005, 2007), and recent work (Sohn et al., 2019) indicates it may host the largest vapor-dominated thermal area in YNP. Yellowstone Lake and areas north of the present-day lake that were formerly part of the lake host the world's largest hydrothermal explosion craters (Morgan et al., 2003), demonstrating that parts of the system have been prone to catastrophic events in the recent past. Constraining the nature and magnitude of Yellowstone

Lake's hydrothermal system and its contribution to the overall Yellowstone geothermal system is important for understanding the output of the world's largest continental geothermal province and for assessment of regional geologic hazards.

Hydrothermal activity within Yellowstone Lake is an ongoing process related to convective-meteoric fluid circulation, with phase separation, fluid accumulation and release of volatiles including CO_2 and H_2S from an actively degassing magma chamber (e.g., Lowenstern & Hurwitz, 2008). Numerous hydrothermal features have been mapped on the lake floor (Morgan et al., 2003, 2007, 2009). They range from individual hydrothermal vents to vent fields and include large (>100- to 2,600-m diameter) hydrothermal explosion craters, vent-lined fissures, gas-emitting (steam, CO_2, H_2S) vents, large venting plumes, hydrothermal domes, sinter deposits, and siliceous spires (Johnson et al., 2003; Morgan et al., 2003, 2007; Shanks et al., 2005, 2007) (Figure 1).

In an effort to characterize the dynamic nature of the lake floor hydrothermal features, a team of researchers embarked in 2016 on a multiyear project funded by the National Science Foundation entitled Hydrothermal Dynamics of Yellowstone Lake (HDYLAKE.org). The project utilized a wide range of marine geophysical, geochemical, and geological techniques to obtain unprecedented spatial and time series data on a sublacustrine hydrothermal system (Sohn et al., 2017). The focus area of study is the northern part of the lake, which is characterized by high heat flow values (Morgan et al., 1977; Smith et al., 2009) and hosts a wide variety of hydrothermal features (Balistrieri et al., 2007; Gemery-Hill et al., 2007; Johnson et al., 2003; Morgan et al., 2003, 2007; Shanks et al., 2005, 2007) (Figure 1). As part of the HD-YLAKE project, a high-resolution magnetic survey was conducted over the northern lake in 2016 using the 7-m-long USGS research vessel *Alamar*. The lake survey was supplemented by a 2016 high-resolution, near-bottom, *REMUS 600* autonomous underwater vehicle (AUV) magnetic survey that focused on an active, 200-m-wide hydrothermal vent field, referred to as the "Deep Hole" (DH), east of Stevenson Island (SI in Figure 1).

High-resolution magnetic surveys of hydrothermal vent systems in the marine environment have revealed distinctive magnetic anomalies associated with active, inactive, and relict hydrothermal vents (e.g., Tivey & Dyment, 2010). At mid-ocean-ridge-hosted vent sites, the typical host rock is highly magnetized basalt, which effectively becomes demagnetized by acidic hydrothermal fluids rising through well-defined upflow zones within the basaltic crust creating punctuated magnetic anomaly lows (e.g., Szitkar et al., 2014; Szitkar & Dyment, 2015; Tivey et al., 2014; Tivey & Johnson, 2002; Zhu et al., 2010). In more felsic environments, such as at back-arc spreading centers and arc volcanoes, the more silica-rich host rock is typically less magnetic and yet zones of reduced magnetization are still observed over hydrothermal areas (e.g., Caratori Tontini et al., 2012; Fujii et al., 2015).

High-resolution magnetic surveys over hydrothermal systems within continental volcanic provinces also reveal distinctive magnetic signals. Negative magnetic anomalies and areas of subdued magnetic signal have been observed over rhyolitic rocks in the Taupo volcanic zone, New Zealand (Caratori Tontini et al., 2016; Hochstein & Soengkono, 1997; Morrell et al., 2011; Studt, 1959) and at Yellowstone National Park (Bouligand et al., 2014; Finn & Morgan, 2002). In most cases, they are attributed to a significant decrease in magnetization due to dissolution and/or transformation of magnetite into weakly magnetized minerals such as hematite or pyrite. Different behaviors have been observed between liquid- and vapor-dominated systems. In the latter case, demagnetization by alteration appears to be absent from the vapor-dominated reservoir. Alteration in subaerial vapor-dominated systems is restricted to the near surface where ground or surface waters mix with acid-sulfate steam-condensate and intensely alter the rock and its magnetic minerals (Bouligand et al., 2019; Hochstein & Soengkono, 1997). Nevertheless, such magnetization differences may be erased through time as a hydrothermal system evolves through several stages of alteration including both vapor- and liquid-dominated phases (Hochstein & Soengkono, 1997). Evidence of these stages may however be present in the alteration mineralogy (Bargar & Muffler, 1982; Larson et al., 2009).

Magnetic anomaly signatures provide useful insight into the subsurface distribution and geometry of hydrothermal upflow zones. The alteration of the magnetic carrier minerals, typically magnetite or titanomagnetite, is a permanent effect so that magnetic anomalies also provide insight into the pattern of hydrothermal circulation integrated over time. In addition to the demagnetization of magnetic minerals by alteration processes, the magnetic response of a section of crust also can be influenced by thermal processes, where minerals, such as magnetite, become nonmagnetic above their Curie temperature of 580°C. In this case,

magnetization loss is only temporary and rocks will become magnetized once they cool below their respective Curie points, but possibly with a significant change in the direction of its remanent magnetization.

The primary objectives of this study are to identify the spatial relationships between hydrothermal activity and magnetic anomalies, provide insight into the temporal nature of the vent activity through the identification of extinct hydrothermal areas, and image subsurface structures that may influence the hydrothermal system and ultimately the thermal state of the region beneath the lake. In this paper, we take a multiscale approach by modeling and interpreting not only the newly collected HD-YLAKE high-resolution lake magnetic survey and AUV survey but also data from a low-altitude aeromagnetic survey flown in 2016 (Finn et al., 2020), and a more regional and higher altitude aeromagnetic survey flown in 1997 (Finn & Morgan, 2002; U.S. Geological Survey, 2000). We also use heat flow data (Smith et al., 2009) to make a first-order estimate of the depth to the Curie isotherm and the base of the magnetized crust as a constraint for the magnetic modeling.

2. Geological Setting

Located in southeastern YNP, the northern basin of the Yellowstone Lake occupies the southeastern portion of the now-collapsed 0.63-Ma Yellowstone caldera created by the eruption of the Lava Creek Tuff (Christiansen, 1984, 2001; Matthews et al., 2015; Morgan et al., 2003; Wotzlaw et al., 2015) (Figure 1). Following collapse of the caldera, rhyolitic lava flows were emplaced within the caldera and along the caldera margins in multiple pulses. A smaller caldera at West Thumb Geyser Basin formed around 160 ka during the last major period of volcanism on the Yellowstone Plateau (Christiansen, 2001) (Figure 1). The region was impacted by two major glaciations that have occurred over the past 160,000 years: the Bull Lake glaciation that peaked around 150 ka and overlapped with periods of recent volcanism (Licciardi & Pierce, 2018; Richmond, 1965) and the Pinedale glaciation that began around 24 ka and receded from the Yellowstone Lake basin at about 14 ka (Licciardi & Pierce, 2008, 2018).

The eastern topographic rim of the 0.63-Ma Yellowstone caldera parallels a segment of the eastern lake shoreline shown in Figure 1. Areas to the west and north of the lake, well inside the caldera, are composed mostly of postcaldera rhyolite flows (Figure 2a) (Christiansen, 2001; Morgan et al., 2007). The steep and rugged Absaroka Range that forms the eastern margin of the lake, outside the caldera margin, is a complex of Tertiary (Eocene) volcanic, mostly andesitic, rocks that represents an earlier and different type of volcanism (Feeley et al., 2002; Prostka, 1973). A thin veneer of extracaldera facies of the 0.63-Ma Lava Creek Tuff laps onto these mountains. Although the Lava Creek Tuff is mostly exposed outside the caldera, it also may compose part of the volcanic basement of the lake (Otis et al., 1977). Based on bathymetry (Morgan et al., 2003), seismic reflection data (Johnson et al., 2003), aeromagnetic data (Finn & Morgan, 2002), and limited sample data collected with a submersible vehicle, the younger rhyolite flows are thought to compose a large portion of the basement of the northern and western half of the lake (Morgan et al., 2003, 2007; Morgan & Shanks, 2005) (Figure 2a). Tertiary volcanic rocks, generally andesitic, are exposed both east and south of the lake margin and likely compose part of the volcanic basement of the lake. Pleistocene glacial deposits mantle the topography of the lake margins; Stevenson, Frank, and Dot Islands; and the lake's volcanic basement. A blanket of fluvial and lacustrine sediments <10 m to ~100 m thick (Johnson et al., 2003; Otis et al., 1977) lie atop the sublacustrine glacial deposits. The eastern central basin of the lake, which is the deepest part of the investigated area (at ~90 m depth), is covered by thick (>100 m) sedimentary deposits (Otis et al., 1977) (Figure 2b) sourced from the Yellowstone River, which enters at the south end of the Southeast Arm of Yellowstone Lake. The only outlet from the lake is located at Fishing Bridge at the northern end of Yellowstone Lake (FB in Figure 1).

The northern lake and its margins have three structural domains that reflect the present-day regional stress fields (Figures 1 and 2a): (1) A set of discontinuous but closely spaced active north-south trending Holocene faults or fissures associated with the extensional system of the Eagle Bay fault zone extends over ~20 km in total length from Fishing Bridge to Eagle Bay (Johnson et al., 2003; Locke et al., 1992; Meyer & Locke, 1986) (Figure 1). Based on the amount of vertical displacement observed on seismic reflection data, the Lake Hotel graben (LHG in Figure 1) is considered a segment of the Eagle Bay fault zone (Johnson et al., 2003). Additionally, the Eagle Bay fault zone might be related to the eastern edge of the older, and now buried, ~ 2.08-Ma Huckleberry Ridge caldera (Christiansen, 2001). (2) A set of northeast

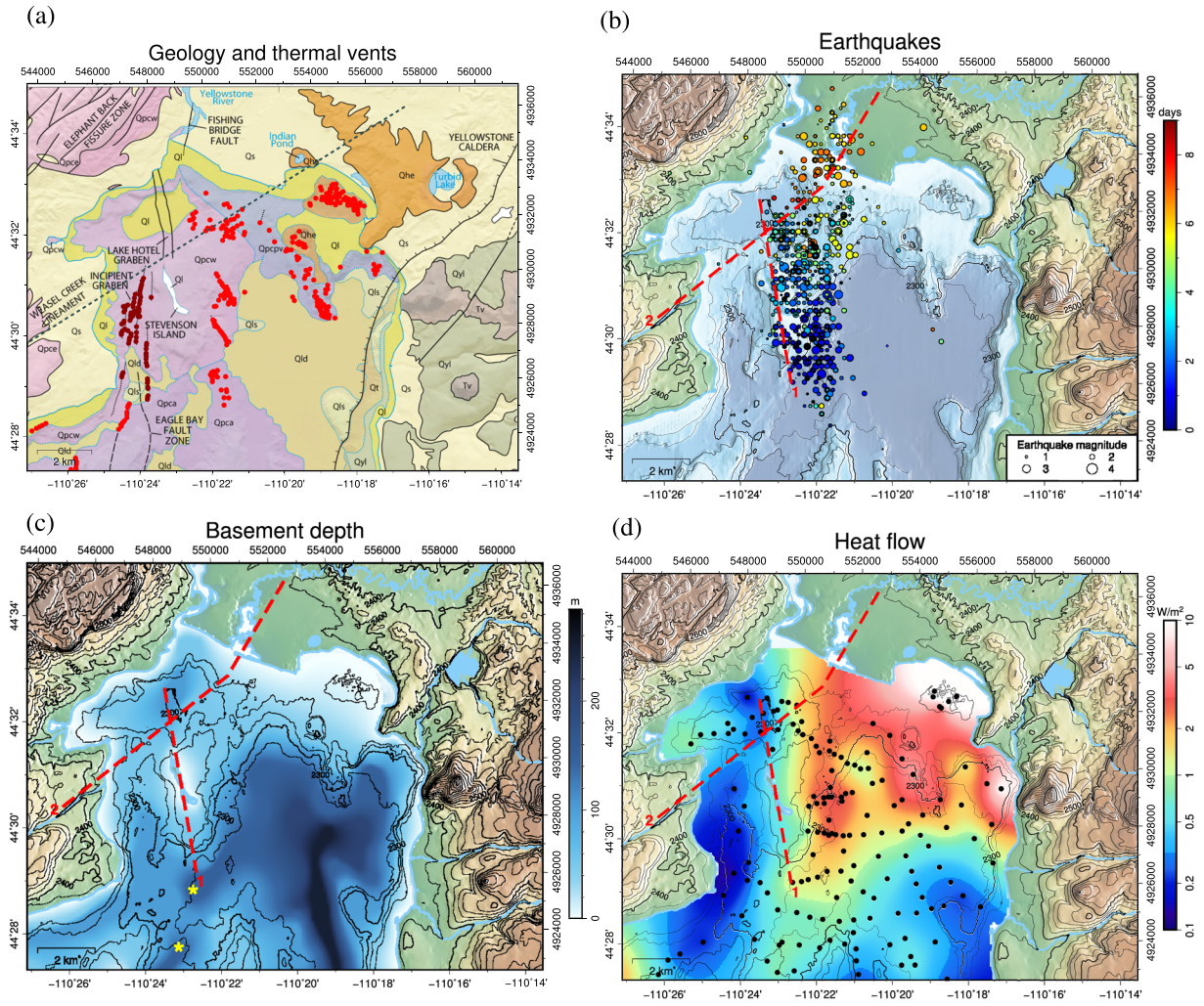

Figure 2. Maps of northern Yellowstone Lake: (a) Geology from Morgan et al. (2007, 2017), (b) depth to basement (below lake surface) digitized and regridded from the original map of Otis et al. (1977) determined from seismic reflection data, (c) distribution of earthquakes (circles) with magnitude >0 during the Yellowstone Lake swarm of earthquakes (27 December 2008 to 7 January 2009; data are from the Yellowstone 3-D catalog from University of Utah (https://quake.utah.edu/regional-info/earthquake-catalogs/yellowstone-3d-catalog); colors indicate time after 27 December 2008, the day of the initial event; size is proportional to magnitude) over topographic map, (d) heat flow, digitized and then regridded from Smith et al. (2009) after interpolating heat flow contours at data locations (black dots). The geological units represented on panel (a) are (ordered with increasing age) as follows: Qs sediments, Ql shallow-lake sediments, Qld deep-lake sediments, Qhe hydrothermal-explosion deposits, Qls landslide deposits, Qt talus and slope deposits, Qpce Elephant Back rhyolite flow, Qpcw West Thumb rhyolite flow, Qpca Aster Creek rhyolite flow, Qpcpv Pelican Creek rhyolite flow, Qyl Lava Creek Tuff, Tv Tertiary volcanic rocks. Fractures and fault are marked on panel (a) by black lines (dashed where approximately located or inferred; dotted where concealed). Red dots are hydrothermal vents and dark red dots are features aligned with fissures discussed in the text. Red dashed lines on panels (b)–(d) are linear magnetic features likely representing faults or fractures. The yellow stars in panel (b) mark a disruption in a paleochannel observed in the basement map. Coordinates of maps in this figure and the following ones are given in longitude and latitude and projected coordinated in UTM12N WGS84.

trending linear structures or fissures are subparallel to the trend of the Elephant Back fissure zone connecting the two tectonically active resurgent domes of Sour Creek (SC) and Mallard Lake (ML) (Figure 1) (Christiansen, 2001; Dzurisin & Yamashita, 1987; Pierce et al., 2007). These fissures appear extensional and related to the active inflation and deflation of the Yellowstone caldera (Dzurisin et al., 1990, 2012; Pelton & Smith, 1979, 1982; Pierce et al., 2007; Wicks et al., 1998, 2006). Between 1926 and 1985, close to 1 m of uplift has occurred along this zone. This regional trend also is reflected in a northeast trending structure that incises the lake bathymetry and lake margin topography from the western shore, along the Weasel Creek lineament (WC), to the northeastern shore, at Storm Point (SP), and into the lower Pelican Valley (PV) (Morgan et al., 2007) (dashed gray line in Figure 1). (3) Locally,

two well-developed and hydrothermally active northwest-trending linear fissures (F1 and F2 on Figure 1) are located east-southeast of Stevenson Island. These fissures host some of the deepest, hottest, and most active hydrothermal vents in Yellowstone Lake, including the Deep Hole site (DH on Figure 1) (Johnson et al., 2003; Morgan et al., 2003; Sohn et al., 2017, 2019). Another set of vents immediately south of these two fissures may reflect a third fissure (F3 on Figure 1).

Active deformation in the lake is supported by evidence of cycles of uplift and subsidence (Dzurisin et al., 1990, 2012; Wicks et al., 1998, 2006) that created multiple lake terraces during the Holocene (Locke et al., 1992; Meyer & Locke, 1986; Pierce et al., 2002, 2007). Seismic activity in YNP and in the lake basin is well documented (e.g., Farrell et al., 2010; Smith et al., 2009). For example, over a 10-day period from December 2008 to January 2009, a swarm of earthquakes propagated from south of Stevenson Island to north of the Lake Hotel graben (Figure 2c) and is interpreted to be the result of the migration of magmatic or hydrothermal fluids (Farrell et al., 2010).

Large variations in heat flow are measured within the lake ranging from ~0.1 W/m^2 in the northwestern part of the lake to over 2 W/m^2 in the northeastern part of the lake (e.g., Smith et al., 2009) (Figure 2d). The area of very high heat flow also coincides with a particularly active hydrothermal system. Expressions of this hydrothermal system include several still-active hydrothermal systems in the Mary Bay (MB) and Elliott's (EC) explosion craters in Yellowstone Lake and at the nearby Turbid Lake (TL) and Indian Pond (IP) explosion craters on land (Figures 1 and 2a). Large hydrothermal domes such as the North Basin hydrothermal dome (NBD in Figure 1) in the lake and at Storm Point (SP) at the lake's northern edge (Figure 1) also are present, along with hundreds of active and inactive hydrothermal vents and inactive siliceous spires (Morgan et al., 2007; Shanks et al., 2007). The accumulation of hydrothermal gas and fluids below a low permeability cap results in the deformation of overlying sediments and formation of domal structures (Johnson et al., 2003; Morgan et al., 2007, 2009).

YNP hosts a wide range of hydrothermal systems, from liquid-dominated alkaline-chloride systems to vapor-dominated systems with acid-sulfate waters (e.g., Bargar & Muffler, 1982; Fournier, 1989; Larson et al., 2009; White et al., 1971). This diversity also is reflected in the systems mapped and sampled in Yellowstone Lake (Balistrieri et al., 2007; Fowler, Tan, Cino, et al., 2019, Fowler, Tan, Luttrell, et al., 2019; Shanks et al., 2005, 2007). Analysis of altered rock samples from U.S. Geological Survey (USGS) drill cores collected within hydrothermal areas from YNP in the late 1960s (White et al., 1975) shows that magnetite, which is the primary carrier of magnetization in unaltered rock samples (e.g., Reynolds, 1977), is partly to completely altered and coexists with secondary weakly or nonmagnetic minerals such as hematite, goethite, and pyrite (Bargar & Beeson, 1984; Bargar & Muffler, 1982). The presence of secondary pyrrhotite, which is usually strongly magnetic, has been occasionally observed in some YNP drill cores but only in low abundance and in restricted parts of the cores (e.g., Bargar & Beeson, 1981; White et al., 1988). At the Deep Hole site, which was the focus of the HD-YLAKE AUV survey, fluid sampling and temperature measurements document a 174°C fluid with a pH of 4.2 that contains 18 wt.% of steam originating from boiling meteoritic water plus volatiles composed of CO_2 and H_2S and is mixed with lake water (Fowler, Tan, Cino, et al., 2019; Tan et al., 2017), indicative of a vapor-dominated system. Push cores collected by submersible at the vent site show that the surficial sediments consist of clast-supported, semilithified, altered mud breccias composed of kaolinite, boehmite, pyrite, and traces of pyrrhotite (Fowler, Tan, Cino, et al., 2019; Fowler, Liu, et al., 2019). The clay sediments likely act as an impermeable cap containing the buoyant vapor-dominated fluids beneath the Deep Hole vent site.

3. Data

The first comprehensive geophysical mapping of Yellowstone Lake occurred in the early 1970s with a series of geophysical campaigns, including seismic reflection and refraction, magnetic methods, heat flow and piston cores, that revealed the basic structure of the lake (Morgan et al., 1977; Otis et al., 1977; Shuey et al., 1977; Wold et al., 1977). Further mapping of heat flow continued in the 1980s (e.g., Smith et al., 2009). An airborne magnetic survey acquired in 1997 (U.S. Geological Survey, 2000) showed a broad magnetic anomaly low in the northeastern part of the lake suggestive of lower crustal magnetization and/or a thinner magnetic layer coinciding with the area of very high heat flow and hydrothermal activity (Finn & Morgan, 2002). Renewed lake mapping from 1999 through 2003 using differential GPS, sonar imaging, seismic reflection, and submersible studies including fluid and solid sampling and photographic documentation (Morgan et al., 2003),

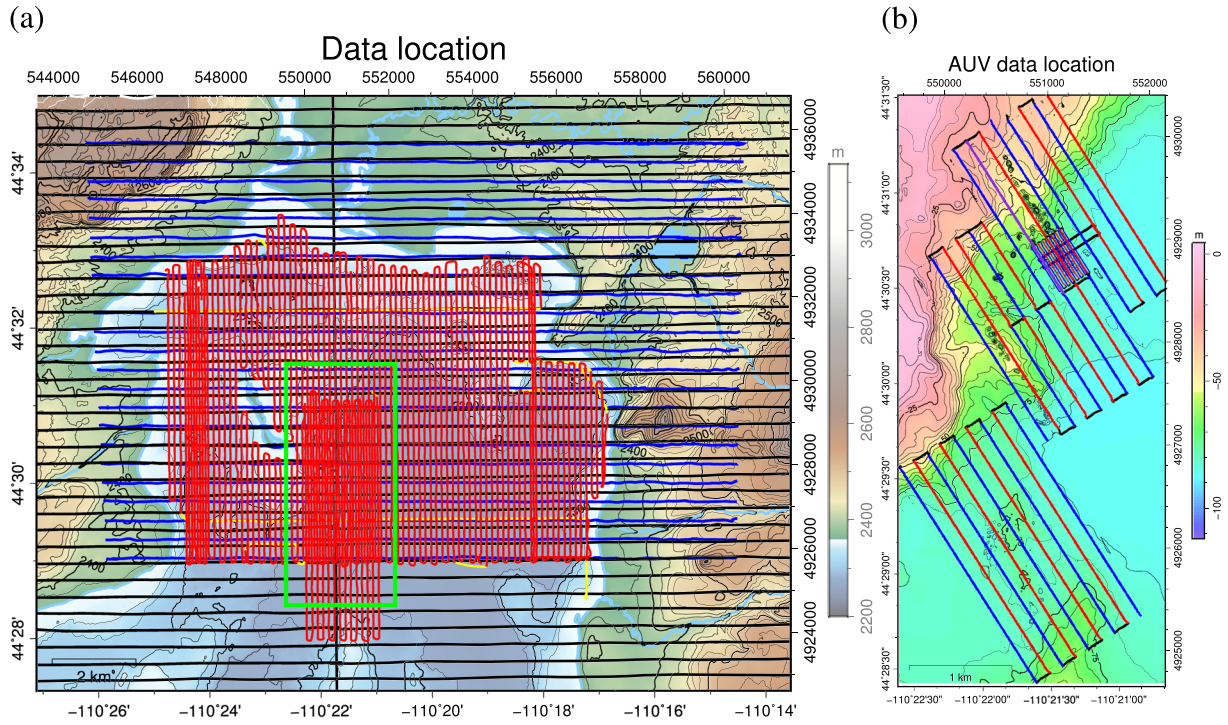

Figure 3. (a) Location of boat (lines in red; small lines and tie-lines not used for the merged grid in yellow) and airborne (2016 in blue and 1997 in black) survey lines over topography. The green rectangle is the outline of panel (b). (b) Location of autonomous underwater vehicle (AUV) lines over bathymetry. Northwestward and southeastward lines are in red and blue, respectively, whereas maneuvers are in black. The line in violet was repeated in both directions. The thick widely spaced lines were acquired at 15 m above the lake floor, and the thin, closely spaced lines were acquired at 7 m above the lake floor.

provided the basis for the first high-resolution comprehensive bathymetric and geologic map of Yellowstone Lake (Morgan et al., 2003, 2007).

For this study, we combine data sets from four different magnetic field surveys acquired at different elevations and with different characteristics (Figure 3): two airborne magnetic surveys, one acquired in 1997 (east-west lines with a 400-m spacing and draped over topography at ~240 m above the lake surface but reaching up to ~600 m above ground on land; U.S. Geological Survey, 2000) and one in 2016 (east-west lines with a 400-m spacing and at an average of ~50 m above ground and of ~33 m over the lake surface), a surface-towed magnetometer lake survey acquired in 2016 (north-south lines with a 120- or 60-m spacing), and an AUV survey acquired near the lake floor (northwest-southeast lines at 15 m above the lake floor with a 150-m spacing and at 7 m above lake floor with a 25-m spacing). Acquisition and processing details are provided in the supporting information (Texts S1 and S2).

The airborne and lake surface data were merged together to produce a single magnetic anomaly grid draped on the topography and at the lake surface (see Text S1 for details). The resulting merged grid was reduced to the pole (Figure 4a) using the standard reduction-to-the-pole (RTP) transformation (e.g., Blakely, 1996) assuming that magnetization is oriented in the direction predicted for a geocentric axial dipole (GAD) field (declination $D = 0°$ and inclination $I = 63°$). Due to the denser line spacing of the survey data over the lake relative to outside, the resulting magnetic grid displays a much more detailed pattern of short-wavelength anomalies over the lake basin (Figure 4a). Magnetic anomalies also were converted into pseudo-gravimetric anomalies (Baranov, 1957), which we used to search for maxima in the horizontal gradient that usually are observed over the edges of magnetic sources (Blakely & Simpson, 1986; Cordell & Grauch, 1985; Phillips, 2007) (Figure S2). We used this analysis to delineate ridges of gradient maxima that extend over several kilometers (see Figure S2 with relatively linear ridges in red and sinuous-shaped ridges in violet) and that may represent, for example, faults or lava flow limits. Finally, the AUV magnetic data were gridded separately—the 15-m altitude survey was gridded with a 50-m spacing while the 7-m altitude survey was gridded with a 10-m spacing after being complemented with the higher-level AUV survey downward continued to the 7-m level (Figure 5).

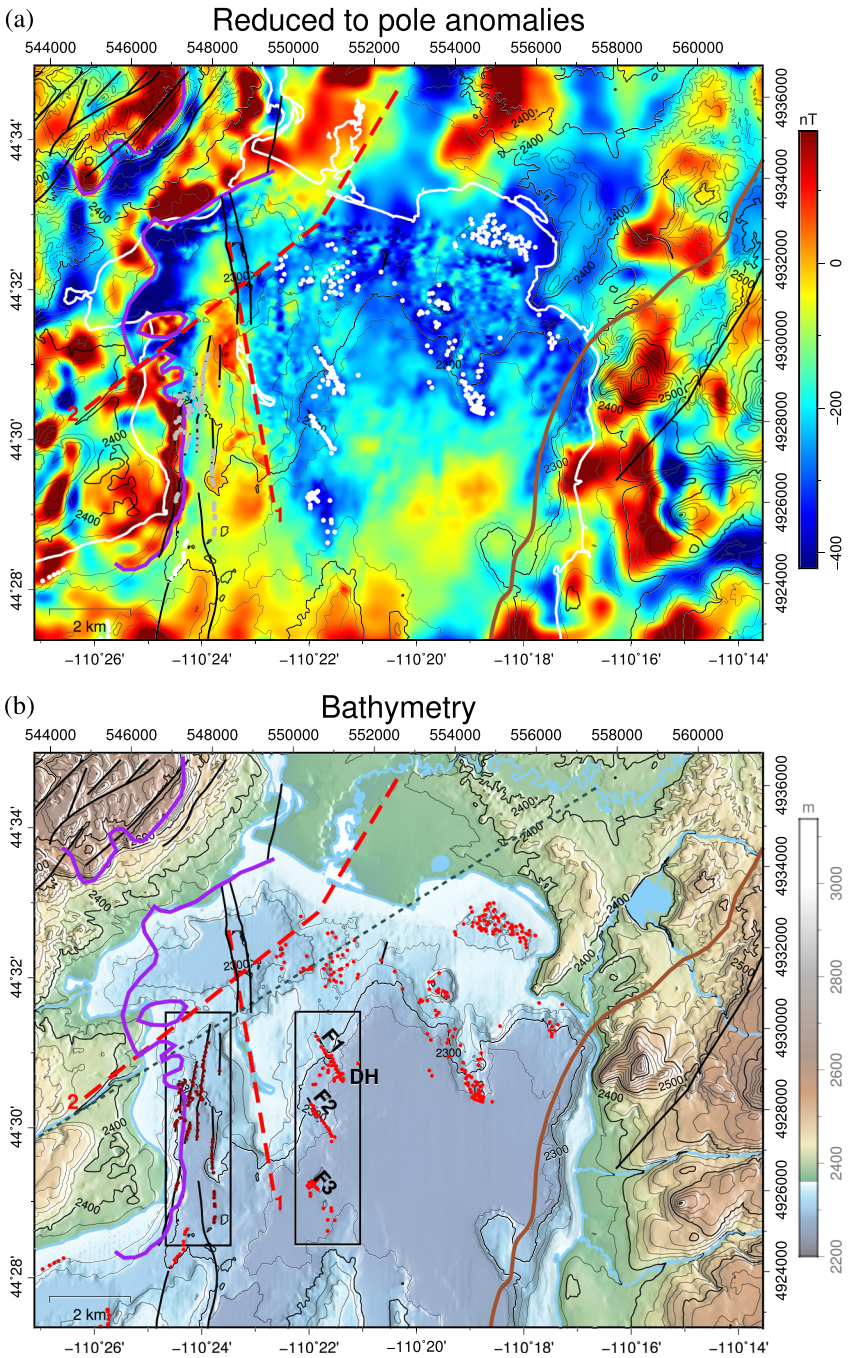

Figure 4. (a) Map of merged reduced-to-the-pole magnetic anomalies, analytically continued to topographic and lake surfaces, (b) map of lake bathymetry with location of faults or fractures from Morgan et al. (2007) (black lines), caldera rim (brown), vents (white dots on panel a and red dots on panel b), features aligned with fissures (gray dots on panel a and dark red dots on panel b), lake outline (white outline on panel a), magnetic linear features (dashed red lines) and sharp sinuous-shaped magnetic gradients (violet lines) that likely reflect leading edges of rhyolite flow units.

The composite merged RTP magnetic anomaly grid (Figure 4a) shows a relatively broad magnetic low over the surveyed northern basin of Yellowstone Lake surrounded by high-amplitude magnetic anomalies to the east, west, and north. This broad magnetic low also is characterized by lower-amplitude horizontal gradients than its surroundings (Figure S2), suggesting lower magnetization contrasts, but is punctuated by local magnetic lows that are either scattered or aligned along linear trends, such as seen immediately east of Stevenson

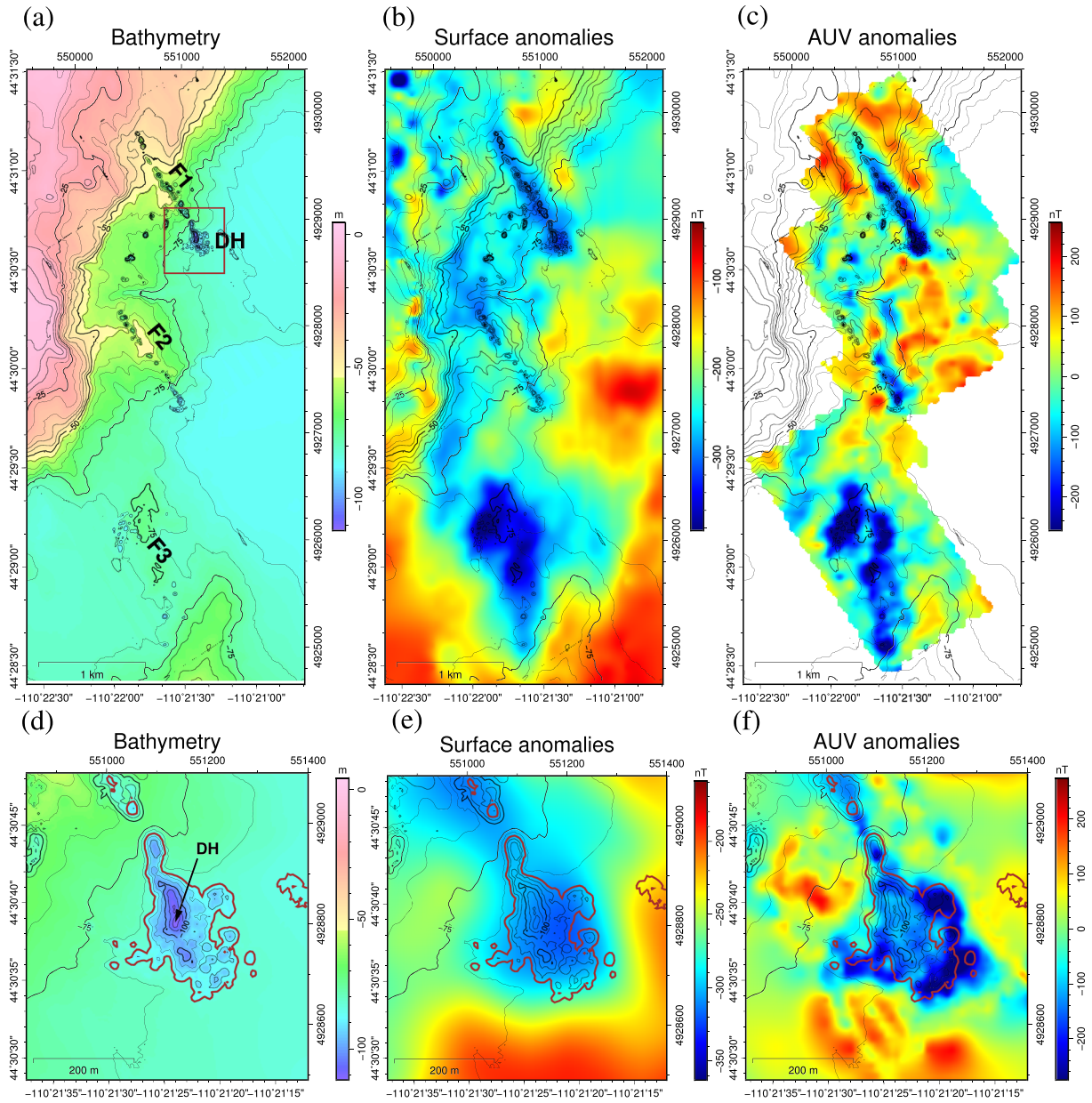

Figure 5. (a) Bathymetry of linear NW to SE trending vent zones east of Stevenson Island, brown box marks the location of panels (d)–(f), (b) lake surface reduced-to-the-pole (RTP) magnetic anomaly showing zones of low magnetism associated with the vent sites in three main areas, (c) AUV 15-m-altitude RTP magnetic anomaly map showing the improved resolution of magnetic lows over the vent areas, (d) high-resolution bathymetry of Deep Hole vent site, (e) lake surface RTP magnetic anomaly over Deep Hole vent site, (f) AUV RTP magnetic anomaly from the 7-m-altitude survey over the Deep Hole vent site showing improvement in the details of the anomalies. The −85 m depth contour line is represented with a thick brown line to delineate the Deep Hole depression. Also reported are the location of three alignments of hydrothermal vents (F1, F2, and F3) and of the Deep Hole vent site (DH).

Island (F1–F3 in Figures 4a and 5b). A striking correlation appears between the distribution of punctuated magnetic lows and lake floor vent depressions in the high-resolution multibeam bathymetry (Morgan et al., 2007) (Figures 4, 5a, and 5b). The discreet linear zones of magnetic lows imaged by the lake surface survey are more clearly resolved in the near-bottom AUV data (Figure 5c). The Deep Hole vent site (DH in Figure 5a), which displays active discharge plumes of gas and hot fluids (Johnson et al., 2003; Sohn et al., 2017, 2019) (Figure 5d), was surveyed by the AUV at 7-m altitude and shows that the high-amplitude magnetic low in the lake surface data (Figure 5e) is composed of a series of punctuated magnetic lows that surround the bathymetric deep hole (Figure 5f).

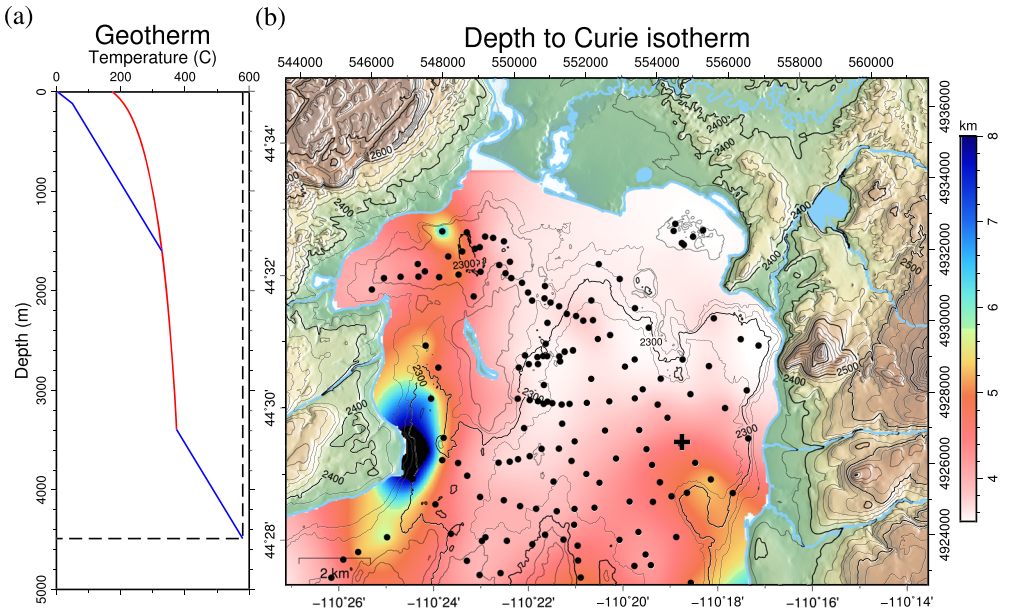

Figure 6. (a) Geotherm deduced from the heat flow estimate located at the black plus symbol on panel (b). At temperature below the boiling temperature (in red), the geotherm (in blue) is linear (conduction with thermal conductivity of 1 W/(m K) in sediments and 2.1 W/(m K) in basement). Below the depth where the geotherm intersects the boiling curve (at ~1.6 km), the geotherm follows the boiling curve up to the critical point. Below the critical point, the geotherm is assumed linear (conduction with thermal conductivity of 2.1 W/(m K)). Note that the geotherm is represented as a function of depth below lake floor and that the boiling temperature at the lake floor is higher than at the lake surface due to pressure from the lake water. (b) Inferred map of the depth to Curie temperature isotherm (580°C) based on heat flow and the modeled geotherm. Location of heat flow data from Smith et al. (2009) is marked by black dots.

4. Analysis and Forward Modeling

We carried out a series of forward models and inversions to characterize the potential sources of the observed magnetic anomalies measured over the lake basin. Details of this analysis are outlined in the supporting information (Texts S3–S5). Summarizing the results briefly, we find that while some local anomalies are likely due to topographic effects—notably Elliott's crater and a small local dome to the southwest of Stevenson Island (see Areas 1 and 2 in Figure S4), the majority of the magnetic signal cannot be attributed to the effect of surface topography or basement topography (Otis et al., 1977).

In order to constrain the base of crustal magnetization, we used heat flow data acquired in Yellowstone Lake from Smith et al. (2009) and digitized their heat flow contour map onto a grid (Figure 2d) to make a first-order approximation of the depth to the 580°C isotherm corresponding to the Curie temperature of magnetite (Hunt et al., 1995) (Figure 6). Although alteration products from magnetite such as hematite or goethite may have a significantly different Curie temperature, we based our estimate on the 580°C isotherm, because we expect magnetite to dominate the signal even when it is in relatively low proportion compared to other weakly magnetic minerals. We followed a method suggested by Morgan et al. (1977), where temperature in the hydrothermal system is assumed to be close to the boiling point and, above and below this hydrothermal zone, heat is transported by 1-D vertical conduction. We estimated the boiling temperature as a function of depth below the lake level using the temperature and density of liquid water as a function of pressure for the saturation condition of pure water (based on data downloaded from https://webbook.nist.gov/) and assuming an atmospheric pressure at lake level (2,358 m) of 0.76 bar and hydrostatic pressure below lake level. Neglecting in situ heat production, we assumed a linear variation in temperature in the sediment (thermal conductivity of 1 W/(m K); Smith et al., 2009) and in the basement (2.1 W/(m K); Morgan et al., 1977) until the boiling condition is reached, then temperature follows the boiling curve up to the critical temperature (~374°C), after which we assumed a linear variation in temperature using a gradient deduced from the surface heat flow (thermal conductivity 2.1 W/(m K)) (Figure 6a). Although heat flow below and above the

hydrothermal system are likely different due to efficient lateral transport of heat in the hydrothermal system, we assumed here they are equal in order to extrapolate temperature at depth below the hydrothermal system and to obtain a first-order estimate of the depth to the 580°C Curie isotherm (Figure 6a).

Curie depth varies from ~3.5 km in the northeastern part of the lake to ~12 km in the western part of the lake (Figure 6b). The depth to the Curie isotherm appears to show very little variation in the northeastern part of the lake, where the geotherm reaches and follows the boiling curve within the inferred hydrothermal reservoir. On the other hand, the Curie isotherm appears to deepen sharply in the western part of the lake, where the geotherm does not reach boiling conditions. Variations in the depth to the Curie isotherm may only cause long wavelength anomalies (i.e., 3.5 km or longer). The removal of the magnetic signal due to magnetization deeper than the Curie temperature isotherm from anomalies due to topography alone (Figure S4b) indeed introduces a long-wavelength magnetic low of ~100 nT, assuming a rock magnetization of 1 A/m (Figure S4d). This low has some similarities with the broad magnetic low of ~300 nT observed in the northeastern part of the lake (Figure S4a), suggesting that this low may be partly due to a thinner magnetic layer in this high heat flow area. Although the predicted and observed magnetic low would be of similar amplitude if we assume a rock magnetization of 3 A/m, their different shapes strongly suggest spatial variations in subsurface magnetization.

We then inverted the magnetic field for a source layer that was bounded by bathymetry at the top and the Curie isotherm at the base. Because of the large variations in the layer thickness (3.5 to 12 km), we did not use the method of Caratori Tontini et al. (2008), as it would have required strong filtering to prevent divergence of the result. Instead, we used an approximate method, where we first inverted magnetization for a layer of constant thickness and then multiplied the result by a corrective factor that varies in x and y and depends of the depth to the top and bottom of the layer. Details of the inversion methodology are given in the supporting information (Text S5). The result, shown in Figures 7 and S6, appears very similar to the more classical equivalent magnetization result obtained for a half space bounded at the top by lake floor bathymetry (Figure S5). Note that because we used the lake bathymetry and not the basement topography as the top of the magnetic layer in the inversions, the resulting equivalent magnetization might be slightly reduced in areas of thick sediment cover (such as in the central basin). However, we note that magnetization lows in Figures 7 and S5c generally do not correlate with areas of thick sediment cover. Magnetization values range from near zero to about 3 A/m along the western shore of the lake. The northeastern part of the lake basin is marked by a broad magnetization low (Figures 7 and S5c) punctuated with discrete lows throughout the hydrothermally active basin including within Mary Bay and Elliott's hydrothermal explosion craters (MB and EC in Figure 1) indicating that the lower magnetic field intensity in this area results from both a thinner magnetic layer and significantly decreased magnetization in the subsurface. A series of linear northwest trending magnetization lows aligned along fissures that host hydrothermal vent sites are also prominent southeast of Stevenson Island.

5. Discussion

5.1. Regional Magnetism of the Northern Lake Basin

The composite magnetic anomaly map (Figure 4a) and the inversion for crustal magnetization (Figure 7) of the northern part of Yellowstone Lake reveal several distinct areas of magnetic character that reflect local subsurface structures of the lake, the influence of the regional and local tectonic stress fields in the vicinity of the lake, the postcaldera lava flows emplaced into a large lake basin, and the impact of high heat flow coupled with subsurface hydrothermal alteration processes.

On a regional scale, the RTP magnetic anomaly map (Figure 4a) shows that the lake basin is bounded by high-amplitude anomalies that are related to the distribution of geologic units (Figure 2a). To the east, the high-amplitude anomalies are related to strongly magnetic Tertiary andesitic rocks and intrusions from the Absaroka Volcanic Supergroup exposed beneath a thin discontinuous veneer of Lava Creek Tuff (Finn & Morgan, 2002). Some of these anomalies extend for a short distance into the lake along the eastern shoreline (Figure 4a). To the north and west of the lake are high-amplitude positive anomalies (Figure 4a) and magnetization values (Figure 7) associated with postcaldera rhyolite lava flows, namely the Elephant Back flow from the northwest and the West Thumb flow from the northwest and west, respectively (Figure 2a).

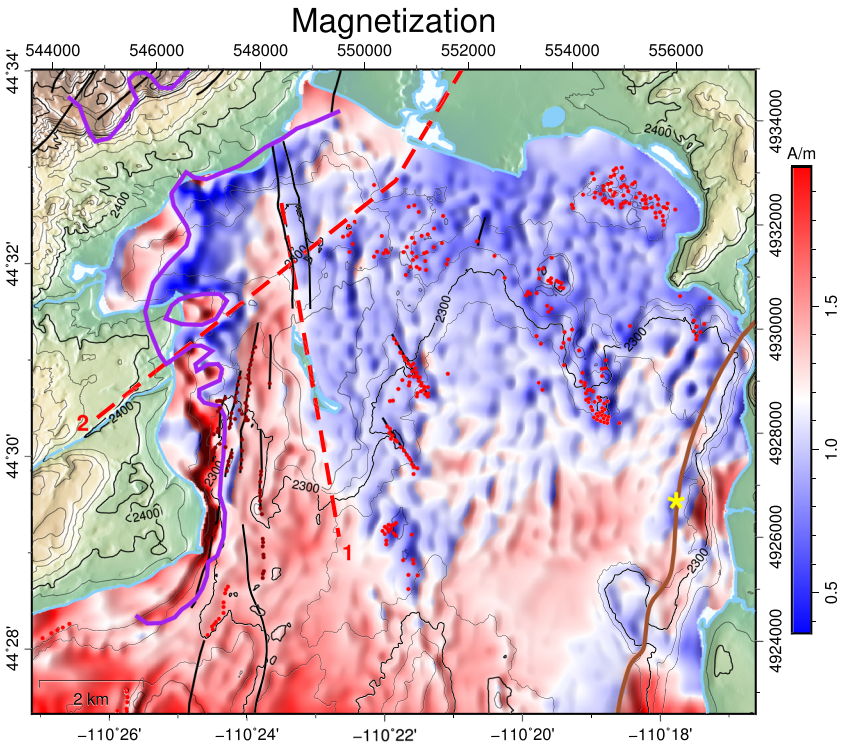

Figure 7. Crustal magnetization inversion result for a layer constrained by bathymetry at the top and by the Curie temperature isotherm at its base. Black lines are faults and fractures from Morgan et al. (2007), the brown line is the 0.63-Ma Yellowstone caldera rim, red dots show the distribution of hydrothermal vents and dark red dots show features aligned with fissures from Morgan et al. (2007) discussed in the text, red dashed lines outline tectonic trends inferred from magnetic anomalies, violet lines represent sharp magnetic gradients that likely reflect leading edges of rhyolite flow units. The yellow star marks a magnetic low coinciding with the 0.63-Ma Yellowstone caldera rim and discussed in the text.

Along the lake's western shore are a set of prominent sinuous-shaped, north-south oriented, high-amplitude, positive magnetization anomalies limited on their eastern side by a sharp gradient (violet line on Figure 7) and a negative anomaly. Such strong magnetization and sharp magnetic gradients also are observed along the leading edge of the Elephant Back flow (Qpce, northwestern corner of Figures 2a and 4a) and recently have been observed by Bouligand et al. (2019) at the margin of an upper flow unit part of the Solfatara Plateau rhyolite flow. We propose that these sinuous-shaped magnetization highs are due to vertical edges of upper flow units of the West Thumb rhyolite flow that are exposed along the western shoreline and partly buried in the lake beneath the lake sediments. Previous measurements of rock samples natural remanent magnetization (NRM) (Finn & Morgan, 2002) from these flows show magnetization in the 3–6 A/m range, which is consistent with the magnetization inversion values of ~3 A/m in this area (Figure 7). The magnetization low located directly to the east of these sinuous-shaped magnetic highs does not correlate with the location of vents, faults, or fracture and might simply reflect a higher sediment thickness in front of the flow edge.

Within the lake basin itself and at the broadest scale, both the airborne and lake surveys show that the north-eastern part of the lake basin, within the caldera, is less magnetic than the surrounding terrain (Figures S1, 4a, and 7). This region displays a distribution of punctuated magnetization lows that closely correlate with the distribution of hydrothermal vents and features in several areas including parts of the Mary Bay and Elliott's hydrothermal explosion craters (MB and EC in Figure 1) and adjacent hydrothermal areas. It should be noted, however, that although all active vents or hydrothermal plumes are associated with a punctuated magnetic low, not all lows coincide with an active vent (Figures 4a and 7). Several of these lows may reflect reduced magnetization due to nonhydrothermal variations, but they also may be the location of now inactive hydrothermal vents, suggesting that significant variations in the location of hydrothermal activity and active

venting may have occurred through time. In addition to the almost ubiquitous distribution of punctuated magnetic lows within this region, significantly lower magnetization is found along two linear 1-km-long, northwest trending zones of fissures (F1 and F2 in Figures 5a–5c and 7) southeast of Stevenson Island that host abundant hydrothermal vents including the Deep Hole vent site (DH). A broader magnetization low to the south has a less distinct bathymetric definition (F3 in Figures 5a–5c and 7). Along the eastern lakeshore, a linear zone of low magnetization also coincides with part of the 0.63-Ma caldera rim (yellow star and brown line in Figure 7), suggesting enhanced hydrothermal alteration along this structure may be used to help refine its exact path (Finn & Morgan, 2002; Morgan et al., 2003, 2007). Collectively, hydrothermal alteration and the shallow Curie isotherm due to high heat flow in the northeastern part of the lake contribute to an overall decrease in magnetic field intensity (Figures 6 and 7). The source of heat is likely a crustal magma reservoir whose top is at a depth of ~3.5–5 km below sea level (i.e., ~6–7.5 km below ground level), as identified on seismic tomography images (Farrell et al., 2014; Husen et al., 2004).

The overall region of low magnetization in the northeastern part of the lake basin is sharply bounded on its western side by a zone of moderate to high magnetization whose approximately north-south trending eastern edge (red dashed line 1 in Figure 7) cuts along Stevenson Island and continues north along the western side of the young and active Lake Hotel graben (<15 ka, Johnson et al., 2003). This edge also coincides with a very steep thermal gradient (Figure 2d) and a sharp deepening of the Curie isotherm to the west (Figure 6) and may indicate a significant structural boundary that limits the hydrothermal circulation prevalent in the northeastern part of the lake. This is further emphasized by the distribution of earthquakes in the 2008–2009 swarm (Figures 2c and 7) that are constrained to the east of this boundary and were interpreted to be related to the migration of magmatic or hydrothermal fluid (Farrell et al., 2010). This boundary also coincides with the contact between two geologic units (Richmond, 1977) on Stevenson Island, with sediments from the Pinedale glaciation to the west against younger sediments to the east, as would be expected for a tectonic structure, although no fault has been mapped on the island. In addition, if we extend this boundary slightly to the south (red dashed line 1 in Figure 2b), it also coincides with a disruption in a paleochannel seen in the basement depth map (yellow stars in Figure 2b; Otis et al., 1977), suggesting that displacement may have occurred across this structure. Finally, given that higher magnetism to the west of this boundary could partly reflect shallower volcanic basement (although not apparent on the depth to basement map, Figure 2b; Otis et al., 1977) and its alignment with the western side of Lake Hotel graben, we propose that this structure was affected by vertical movements with the western side moving up with respect to its eastern side (Johnson et al., 2003).

The west side of this moderate to high magnetization zone (Figure 7) coincides with a series of young or reactivated, extension-related faults and fissures along a 10-km-long, north-to-south trend that are part of the ~20-km-long Eagle Bay fault zone (Morgan et al., 2007). It has been suggested that this fault zone is a possible boundary or caldera wall of the 2.08-Ma Huckleberry Ridge caldera (Christiansen, 2001; Morgan et al., 2003). In contrast to the northeastern part of the basin, this area has relatively low heat flow values and shows no obvious magnetic lows. Although hydrothermal vents were initially mapped along the north–south trending fissures from depressions observed in the bathymetry (dark red dots in Figures 1 and 4b) (Morgan et al., 2003, 2007), exploration of this area with a submersible ROV found no active hydrothermal vents or evidence of hydrothermal alteration. Given the absence of magnetization lows (Figure 7) and after reinspection of the bathymetry, which shows a much smoother morphology along these fissures than along the vent alignments located southeast of Stevenson Island (Figure S8), we conclude that this area does not show any evidence of past or active hydrothermal vents. The northeast-trending Weasel Creek lineament (WC in Figures 1 and 4), identified by Morgan et al. (2003, 2007) in the lake floor bathymetry and lake margin topography and paralleling the general trend of the Elephant Back fissure zone, appears to coincide with a trend in the magnetic gradient (red dashed line 2 in Figures S2, 4, and 7) that intersects the block of moderate to high magnetization anomalies.

The broad magnetic field intensity and magnetization low in the northeastern part of the lake is bounded to the south by a gradual shift to more magnetized lake floor and higher magnetic field intensity (Figures 4 and 7). The magnetic character of this area, which has much lower heat flow (Figure 2d) and shows no evidence for hydrothermal activity (Figure 2a), most likely reflects a deeper Curie temperature isotherm and the absence of hydrothermal alteration. It might also relate to the presence of the Aster Creek rhyolite flow extending farther north and east into the basin beneath a relatively thick sediment cover (Morgan

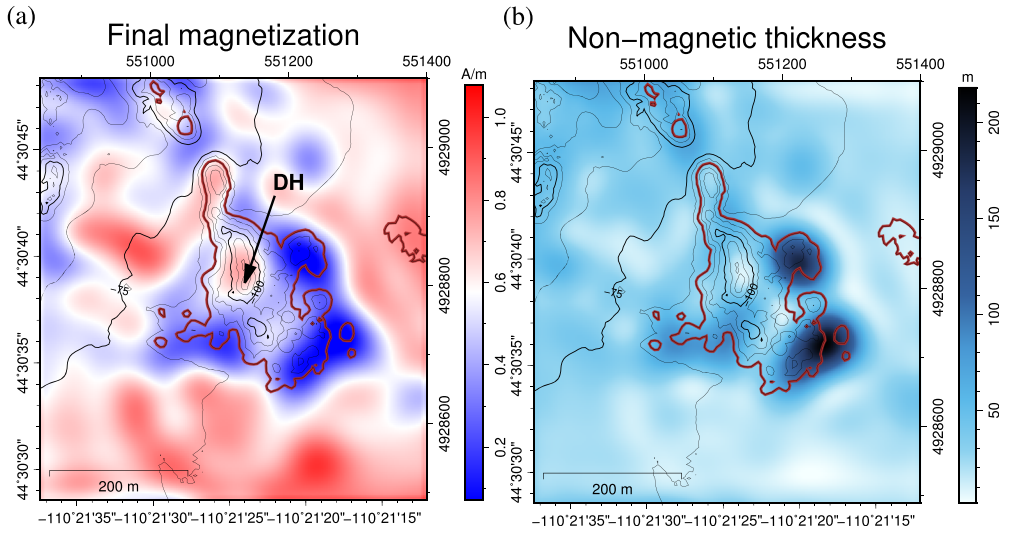

Figure 8. AUV magnetic analysis plot of the Deep Hole area (located by a brown square in Figure 5a): (a) Inverted equivalent magnetization of AUV magnetic survey at ~7 m above lake floor assuming a half space below bathymetry, (b) computed thickness of nonmagnetic material below bathymetry. Contours are bathymetric depths, 5-m contour interval. The −85-m depth contour line is represented with a thick brown line to delineate the Deep Hole depression. Also reported is the location of the center of the Deep Hole vent site (DH).

et al., 2007) (Figures 2 and 7), although given the gradual nature of the magnetic transition this is less likely.

Overall, the distribution of hydrothermal activity and punctuated magnetization lows are influenced by the three prevailing extensional stress fields and include the following: (1) a north–south trend associated with the Eagle Bay fault zone, which may be a part of the collapsed caldera wall of the 2.08-Ma Huckleberry Ridge caldera; (2) a more local northwest trend reflected in lineaments F1, F2, and F3 (Morgan et al., 2003); and (3) a weakly defined regional northeast trend associated with the Weasel Creek-Storm Point lineament, which is subparallel to the Elephant Back fissure zone and related to the widespread deformation of the Yellowstone caldera. While the local northwest trending stress field is host to abundant hydrothermal activity that destroys basement magnetization (as observed directly east of Stevenson Island), the north-south trending fabric (red dashed line 1 in Figures 4 and 7a) seems to be a barrier to hydrothermal fluids as it bounds the area of ubiquitous punctuated magnetic lows to the west and northwest.

5.2. Magnetism of the Deep Hole Hydrothermal Site

One of the goals of the magnetic survey was to investigate the relationship between magnetism and the hydrothermal systems beneath the lake. The hydrothermal venting southeast of Stevenson Island is marked by two prominent northwest trending, linear, and narrow zones of magnetic lows that coincide with fissures that host hydrothermal vents (F1 and F2 in Figures 1 and 4), the Deep Hole site being the most prominent (Figures 4a and 4b). While part of these magnetic low signatures can be explained by the topographic effect of the vents, the persistence of zones of reduced magnetization in the inversion result indicates that hydrothermal activity has had a demagnetizing effect upon the subsurface crust (Figures 5 and 7). The near-bottom AUV magnetic survey over the Deep Hole hydrothermal vent field provides more details on possible demagnetization processes (see Text S6 for details). The magnetic low observed over the Deep Hole differs from the predicted bathymetric anomalies (Figures 5f, S7a, and S7b), and the equivalent magnetization inversion suggests discrete zones of low magnetization (Figures 8a and S7e). We estimate a minimum volume of weakly magnetized material by assuming the presence of nonmagnetic material at the surface and inverting for the base of this nonmagnetic material starting from the lake floor bathymetry and iteratively modifying the thickness following the method of Bouligand et al. (2014) (Figures 8b and S7h). Such nonmagnetic material could either be rhyolites whose magnetization was destroyed by hydrothermal alteration or a combination of altered rhyolite and weakly magnetic lake bottom sediments. We estimate the volume of nonmagnetic material to be ~0.012 km^3 with a maximum thickness of ~220 m.

Furthermore, we find that the magnetization is reduced around the outer edges of the Deep Hole vent site, but not at the center of the vent field (Figure 8), where gas flux dominates and heat flow is at a maximum (Fowler, Tan, Cino, et al., 2019; Sohn et al., 2019). Such an outer ring of decreased magnetization has not been previously observed over any of the terrestrial vapor-dominated venting areas of YNP, possibly due to the lower spatial resolution of previously available magnetic data. However, a recent high-resolution ground magnetic survey of the on-land, vapor-dominated Solfatara Plateau thermal area in YNP (Bouligand et al., 2019) showed that a decrease in magnetization was restricted to the near surface and in a few areas offset from the buoyant gas and heat plume.

Potential insight into this unexpected pattern of demagnetization comes from studies in the Taupo volcanic zone, New Zealand, showing that magnetite is stable in the core of vapor-dominated systems, except in the near surface, where the vapor condenses and becomes strongly acidic due to oxidation of H_2S by O_2 to H_2SO_4 (sulfuric acid) that pervasively alters host rocks (Hochstein & Soengkono, 1997). However, in contrast to subaerial systems, the amount of acidity produced by H_2S oxidation in sublacustrine hydrothermal systems is very small due to limited dissolved oxygen supply. Studies of Yellowstone Lake waters show 8.2–10.8 mg/kg dissolved O_2(aq) (i.e., ~0.001 wt.%) (Knight, 1975) in comparison to 22% O_2(g) in the air. Because of the limited oxygen supply, acid-sulfate alteration is not a likely explanation for the destruction of magnetite around the Deep Hole vent site. In fact, Balistrieri et al. (2007), Fowler, Tan, Cino, et al. (2019), and Tan et al. (2017) have shown that acidity in vent fluids is due to dissolved CO_2.

We describe here three scenarios that could explain the contrast between the outer and central parts of the Deep Hole vent site displaying enhanced and limited destruction of magnetite, respectively. In one scenario, the lack of oxygen mixing into the hydrothermal fluid in the central part of the vapor-dominated upflow zone could strongly limit magnetite (mt) oxidation to hematite (hm) by the following oxidation (redox) reaction (Equation 1):

$$2\ Fe_3O_4(mt) + 0.5\ O_2(aq) = 3\ Fe_2O_3(hm) \quad (1)$$

This suggestion is reasonable given the relatively low concentration of O_2(aq) in lake water and the difficulty of lake water to egress into the central parts of the active vapor-dominated hydrothermal upflow zone. A second more likely possibility is that magnetite reacts by a nonoxidative process (Ohmoto, 2003; Zhao et al., 2018) as follows (Equation 2):

$$Fe_3O_4\ (mt) + 2H^+ = Fe_2O_3\ (hm) + Fe^{2+} + H_2O \quad (2)$$

In this case, the rate-limiting step is removal of Fe^{2+} by the hydrothermal fluids. This requires liquid, not vapor, to transport dissolved iron, and this is most likely to occur around the flanks of the hydrothermal system where condensation and mixing with ambient lake-derived waters occurs. A third scenario is that some of the magnetite may be destroyed by sulfidation to pyrite (py) by H_2S-rich fluids as follows (Equation 3):

$$Fe_3O_4(mt) + 6H_2S(aq) + O_2(aq) = 3FeS_2(py) + 6H_2O \quad (3)$$

This process requires H_2S and O_2, and both are likely present in the mixing zone around the periphery of the hydrothermal system, whereas only H_2S, CO_2, and steam are present in the center of the upflow zone. This scenario is consistent with results from Fowler, Liu, et al. (2019) and Fowler, Tan, Luttrell, et al. (2019) who have demonstrated the formation of abundant pyrite and trace amounts of pyrrhotite in the intensely altered surficial sediments collected by push cores in the Deep Hole vapor-dominated hydrothermal vent area.

Given these possibilities, we hypothesize that demagnetization in the outer zone is due to hydrothermal alteration of the host rock as a consequence of condensation of vapor as it mixes with lake water (Fowler, Tan, Cino, et al., 2019; Tan et al., 2017), which favors magnetite conversion to hematite or pyrite (Equations 2 and 3). In contrast, the vapor-dominated reducing fluids rising in the center of the vent site are less able to alter magnetite either by oxidation or nonredox removal of Fe^{2+} (Equations 1 and 2), but still might produce some sulfidation of magnetite to pyrite (Equation 3). The overall process is summarized in cross section (Figure 9), which shows decreasing temperature away from the vapor-dominated upflow zone, the cap of altered mud that contains the vapor zone, and the condensation/mixing zone around the

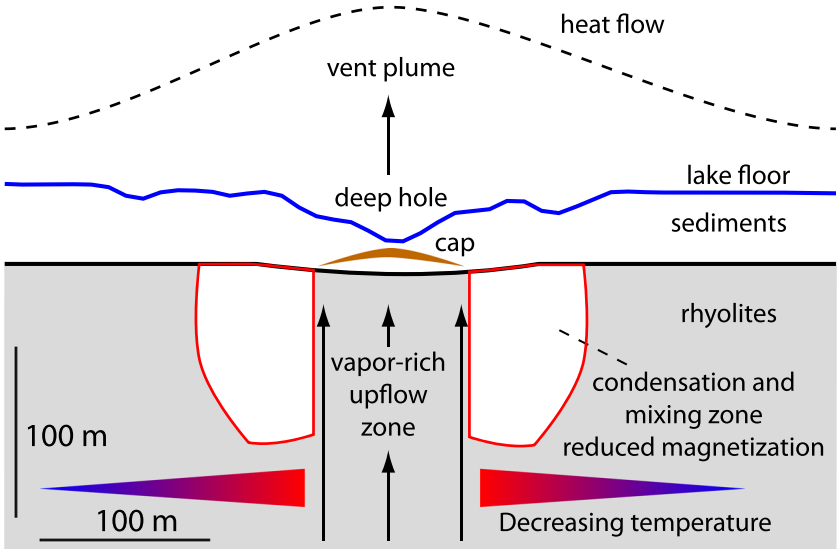

Figure 9. Schematic diagram showing a cross section of the Deep Hole hydrothermal site with a central upflow zone of vapor-dominated fluid where alteration of magnetic minerals is limited compared to the surrounding zones of condensation/mixing where hydrothermal alteration is enhanced and results in decreased magnetization. A semi-impermeable cap composed of kaolinite-boehmite altered mud (Fowler, Tan, Cino, et al., 2019) overlies the upflow zone within the sediments.

periphery where alteration of magnetite is intense. The demagnetization pattern at the Deep Hole also could be a transitory pattern that eventually will be followed by a more complete demagnetization of the vent site over time.

6. Conclusions

Detailed high-resolution magnetic surveys of the northern basin of Yellowstone Lake define several regions within the lake that have a distinct magnetization character:

1. Lower values of magnetic field intensity are prevalent in the northeastern part of the 2016 survey area and reflect the influence of a significant heat source imaged through seismic tomography (Farrell et al., 2014; Husen et al., 2004) and which is at relatively shallow (3.5–5 km below sea level) depths. Overall, the depth to the Curie isotherm is estimated to be ~3.5 km below the ground level (i.e., ~1 km below sea level) in this northeastern part of the lake. This area hosts abundant and varied hydrothermal features and we find a striking correlation in the distribution of magnetic low anomalies with the observation of hydrothermal plume activity. Modeling suggests that this magnetic low region is the result of both a shallow Curie isotherm thinning the source layer and hydrothermally demagnetized rock due to high heat flow and circulation of hydrothermal fluids and gases. We evaluate the total area impacted by hydrothermal activity, as defined by our magnetic inversion, to be ~14 km^2 (corresponding to areas with magnetization lower than 0.9 A/m in Figure 7).
2. The lake basin is surrounded by strong magnetic anomalies on the eastern shore related to the Tertiary Absaroka volcanic range, to the northwest by postcaldera Elephant Back and West Thumb rhyolite flows, and to the south and west by the Aster Creek rhyolite flow. Particularly strong, sinuous-shaped, north striking magnetic anomalies are likely indicative of upper flow unit fronts of the West Thumb rhyolite flow that terminate beneath the western lake edge. Along the southern boundary of the magnetic map and in the central lake basin, magnetization gradually increases to moderate values, which is likely due to the lower heat flow and the absence of hydrothermal activity.
3. Moderate magnetization is found in a block that encompasses Stevenson Island and the western boundary of the Lake Hotel graben. This block is marked by north-south trending fissures and faults that show no obvious hydrothermal activity or magnetic lows and has low heat flow. Although hydrothermal vents were initially mapped from bathymetry along these fissures, the relatively smooth morphology of these fissures and the absence of magnetic lows suggest no evidence of vent activity in this area. The eastern

edge of the block marks a steep gradient in heat flow. We suggest that this is a significant structural feature that restricts hydrothermal circulation to the northeast basin region. This feature may be an edge from the topographic margin of the 2.08-Ma Huckleberry Ridge caldera.

4. Detailed AUV magnetic surveys of the active Deep Hole hydrothermal vent site reveal a surprising distribution of reduced magnetization around the outer ring of the Deep Hole vent site, while the central portion is somewhat more magnetic. We interpret the reduced magnetization as the result of demagnetization associated with hydrothermal alteration and hypothesize that the vapor-dominated reducing fluid that is ascending at the center of the vent zone is less able to alter magnetite either by oxidation or nonredox removal of Fe^{2+} (Equations 1 and 2), but still might produce some sulfidation of magnetite to pyrite (Equation 3). In contrast, the outer ring represents an area of enhanced alteration due to condensation of the vapor and mixing with lake water, which favors magnetite conversion to hematite or pyrite (Equations 2 and 3).

Data Availability Statements

The lake surface and AUV magnetic survey data and the magnetic grid are publicly archived under the HD-YLAKE project at the Marine Geoscience Data System (http://www.marine-geo.org/index.php) hosted at the Lamont Doherty Earth Observatory of Columbia University. The link to the USGS 2016 airborne survey is this site (https://www.sciencebase.gov/catalog/item/5d35fe69e4b01d82ce8a61d1).

Acknowledgments

The lake surface and AUV magnetic data were acquired under National Park Service research permit YELL-2016-SCI-7018 and the 2016 aeromagnetic data under research permit YELL-2016-SCI-7056. We thank Sarah Haas, Stacey Gunther, Erik Oberg, Annie Carlson, and Patricia Bigelow at the Yellowstone Center for Resources for assistance with permitting and logistics, Ranger Jackie Sene for assistance with logistics and safety at Bridge Bay, Bob Gresswell for providing us with the U.S. Geological Survey (USGS) boat *Alamar*, the boat pilot Nick Heredia, and Robert Harris and Shaul Hurwitz for fruitful discussions. We are very thankful to Ocean Floor Geophysics (Brian Claus and Steve Bloomer) who provided the magnetometer for the AUV survey and preprocessed the data, and to the REMUS 600 team (Greg Packard and Greg Kurras) for operating and optimizing the AUV during lake operations. Data from the Newport and Boulder observatories were used to process the survey data. We thank the USGS Geomagnetism Program for supporting their operation and INTERMAGNET for promoting high standards of magnetic observatory practice (www.intermagnet.org). This research was funded by the National Science Foundation's Integrated Earth Systems program EAR-1516361 (HD-YLAKE project), USGS Mineral Resource and Volcano Hazard Programs, and benefited from major in-kind support from the USGS Yellowstone Volcano Observatory. Maurice Tivey was supported under National Science Foundation Grant OCE-1557455. During the course of this study, Claire Bouligand was a visiting scientist at the USGS in Menlo Park, California, USA, benefited from a delegation to Centre National de la Recherche Scientifique (CNRS), and received funding from CNRS-INSU program SYSTER. ISTerre is part of Labex OSUG@2020 (ANR10 LABX56). Any use of trade, firm, or product names is for descriptive purposes and does not imply endorsement by the U.S. Government.

References

Balistrieri, L. S., Shanks, W. C. III, Cuhel, R. L., Aguilar, C., & Klump, J. V. (2007). The influence of sublacustrine hydrothermal vents on the geochemistry of Yellowstone Lake. In L. A. Morgan (Ed.), *Integrated geoscience studies in the greater Yellowstone area—Volcanic, tectonic, and hydrothermal processes in the Yellowstone Geoecosystem*, *U.S. Geological Survey Professional Paper 1717* (pp. 169–199). Reston, VA: U.S. Geological Survey. Retrieved from https://pubs.usgs.gov/pp/1717/downloads/pdf/p1717F.pdf

Baranov, V. (1957). A new method for interpretation of aeromagnetic maps: Pseudo-gravimetric anomalies. *Geophysics*, *22*, 359–383. https://doi.org/10.1190/1.1438369

Bargar, K. E., & Beeson, M. H. (1981). Hydrothermal alteration in research drill hole Y-2, Lower Geyser Basin, Yellowstone National Park, Wyoming. *American Mineralogist*, *66*, 473–490.

Bargar, K. E., & Beeson, M. H. (1984). *Hydrothermal alteration in research drill hole Y-6, Upper Firehole River, Yellowstone National Park, Wyoming, U.S. Geological Survey Professional Paper 1054-B* (pp. 1-24). https://doi.org/10.3133/pp1054B

Bargar, K. E., & Muffler, L. J. P. (1982). Hydrothermal alteration in research drill hole Y-11 from a vapor-dominated geothermal system at Mud Volcano, Yellowstone National Park, Wyoming. *Thirty-Third Annual Field Conference, Wyoming Geological Association Guidebook*, 139–152.

Blakely, R. J. (1996). *Potential theory in gravity and magnetic applications* (p. 464). Cambridge: Cambridge University Press. https://doi.org/10.1017/CBO9780511549816

Blakely, R. J., & Simpson, R. W. (1986). Approximating edges of source bodies from magnetic or gravity anomalies. *Geophysics*, *51*, 1494–1498. https://doi.org/10.1190/1.1442197

Bouligand, C., Glen, J. M. G., & Blakely, R. J. (2014). Distribution of buried hydrothermal alteration deduced from high-resolution magnetic surveys in Yellowstone National Park. *Journal of Geophysical Research: Solid Earth*, *119*, 2595–2630. https://doi.org/10.1002/2013JB010802

Bouligand, C., Hurwitz, S., Vandemeulebrouck, J., Byrdina, S., Kass, M. A., & Lewicki, J. L. (2019). Heat and mass transport in a vapor-dominated hydrothermal area in Yellowstone National Park, USA: Inferences from magnetic, electrical, electromagnetic, subsurface temperature, and diffuse CO_2 flux measurements. *Journal of Geophysical Research: Solid Earth*, *124*, 291–309. https://doi.org/10.1029/2018JB016202

Caratori Tontini, F., Cocchi, L., & Carmisciano, C. (2008). Potential-field inversion for a layer with uneven thickness: The Tyrrhenian Sea density model. *Physics of the Earth and Planetary Interiors*, *166*(1–2), 105–111. https://doi.org/10.1016/j.pepi.2007.10.007

Caratori Tontini, F., de Ronde, C. E., Yoerger, J. D., Kinsey, J., & Tivey, M. (2012). 3-D focused inversion of near-seafloor magnetic data with application to the Brothers volcano hydrothermal system, Southern Pacific Ocean, New Zealand. *Journal of Geophysical Research*, *117*, B10102. https://doi.org/10.1029/2012JB009349

Caratori Tontini, F., de Ronde, C. E. J., Scott, B. J., Soengkono, S., Stagpoole, V., Timm, C., & Tivey, M. (2016). Interpretation of gravity and magnetic anomalies at Lake Rotomahana: Geological and hydrothermal implications. *Journal of Volcanology and Geothermal Research*, *314*, 84–94. https://doi.org/10.1016/j.jvolgeores.2015.07.002

Christiansen, R. L. (1984). Yellowstone magmatic evolution: Its bearing on understanding large-volume explosive volcanism. In *Explosive volcanism: Inception, evolution, and hazards* (pp. 84–95). Washington, DC: National Academy Press. https://doi.org/10.17226/18602

Christiansen, R. L. (2001). *The Quaternary and Pliocene Yellowstone Plateau volcanic field of Wyoming, Idaho, and Montana, U.S. Geological Survey Professional Paper 729-G* (pp. 1-145). https://doi.org/10.3133/pp729G

Christiansen, R. L., Lowenstern, J. B., Smith, R. B., Heasler, H., Morgan, L. A., Nathenson, M., et al. (2007). *Preliminary assessment of volcanic and hydrothermal hazards in Yellowstone National Park and vicinity, U.S. Geological Survey Open-File Report 2007–1071* (pp. 1–94). Retrieved from http://pubs.usgs.gov/of/2007/1071/

Cordell, L., & Grauch, V. J. S. (1985). Mapping basement magnetization zones from aeromagnetic data in the San Juan Basin, New Mexico. In *The utility of regional gravity and magnetic anomaly maps* (pp. 181–197). Tulsa, OK: Society of Exploration Geophysicists. https://doi.org/10.1190/1.0931830346.ch16

Dzurisin, D., Savage, J. C., & Fournier, R. O. (1990). Recent crustal subsidence at Yellowstone caldera, Wyoming. *Bulletin of Volcanology*, *52*(4), 247–270. https://doi.org/10.1007/BF00304098

Dzurisin, D., Wicks, C. W., &Poland, M. P. (2012). *History of surface displacements at the Yellowstone caldera, Wyoming, from leveling surveys and InSAR observations, 1923–2008 U.S. Geological Survey Professional Paper 1788, v. 1.1* (pp. 1-68). Retrieved from http://pubs.usgs.gov/pp/1788/

Dzurisin, D., & Yamashita, K. M. (1987). Vertical surface displacements at Yellowstone caldera, Wyoming, 1976–1986. *Journal of Geophysical Research*, *92*(B13), 13,753–13,766. https://doi.org/10.1029/JB092iB13p13753

Farrell, J., Smith, R. B., Husen, S., & Diehl, T. (2014). Tomography from 26 years of seismicity revealing that the spatial extent of the Yellowstone crustal magma reservoir extends well beyond the Yellowstone caldera. *Geophysical Research Letters*, *41*, 3068–3073. https://doi.org/10.1002/2014GL059588

Farrell, J., Smith, R. B., Taira, T. A., Chang, W. L., & Puskas, C. M. (2010). Dynamics and rapid migration of the energetic 2008–2009 Yellowstone Lake earthquake swarm. *Geophysical Research Letters*, *37*, L19305. https://doi.org/10.1029/2010GL044605

Feeley, T. C., Cosca, M. A., & Lindsay, C. R. (2002). Petrogenesis and implications of calc-alkaline cryptic hybrid magmas from Washburn volcano, Absaroka Volcanic Province, USA. *Journal of Petrology*, *43*, 663–703. https://doi.org/10.1093/petrology/43.4.663

Finn, C. A., Bedrosian, P. A., & Bloss, B. R. (2020). *Airborne electromagnetic and magnetic survey, Yellowstone National Park, 2016*. U.S. Geological Survey. https://doi.org/10.5066/P9MCJ9B6

Finn, C. A., & Morgan, L. A. (2002). High-resolution aeromagnetic mapping of volcanic terrain, Yellowstone National Park. *Journal of Volcanology and Geothermal Research*, *115*(1–2), 207–231. https://doi.org/10.1016/S0377-0273(01)00317-1

Fournier, R. O. (1989). Geochemistry and dynamics of the Yellowstone National Park hydrothermal system. *Annual Review of Earth and Planetary Sciences*, *17*, 13–53. https://doi.org/10.1146/annurev.ea.17.050189.000305

Fournier, R. O., White, D. E., & Truesdell, A. H. (1975). *Convective heat flow in Yellowstone National Park* (pp. 731–739). Paper presented at Proceedings of the Second United Nations Symposium on the Development and Use of Geothermal Resources.

Fowler, A. P., Liu, Q., Huang, Y., Tan, C., Volk, M., Shanks, W. C., & Seyfried, W. E. (2019). Pyrite $\delta^{34}S$ and $\Delta^{33}S$ constraints on sulfur cycling at sublacustrine hydrothermal vents in Yellowstone Lake, Wyoming, USA. *Geochimica et Cosmochimica Acta*, *265*, 148–162. https://doi.org/10.1016/j.gca.2019.09.004

Fowler, A. P., Tan, C., Cino, C., Scheuermann, P., Volk, M. W., Shanks, W. C., & Seyfried, W. E. (2019). Vapor-driven sublacustrine vents in Yellowstone Lake, Wyoming, USA. *Geology*, *47*(3), 223–226. https://doi.org/10.1130/G45577.1

Fowler, A. P., Tan, C., Luttrell, K., Tudora, A., Scheuermann, P., Shanks, W. C. P. III, & Seyfried, W. E. Jr. (2019). Geochemical heterogeneity of sublacustrine hydrothermal vents in Yellowstone Lake, Wyoming. *Journal of Volcanology and Geothermal Research*, *386*, 106,677. https://doi.org/10.1016/j.jvolgeores.2019.106677

Friedman, I., & Norton, D. R. (2007). Is Yellowstone losing its steam?—Chloride flux out of Yellowstone National Park. In L. A. Morgan (Ed.), *Integrated geoscience studies in the greater Yellowstone area, Volcanic, hydrothermal, tectonic processes in the Yellowstone geoecosystem*, *U.S. Geological Survey Professional Paper 1717* (pp. 272–297). Reston, VA: U.S. Geological Survey. https://pubs.usgs.gov/pp/1717/downloads/pdf/p1717I.pdf

Fujii, M., Okino, K., Honsho, C., Dyment, J., Szitkar, F., Mochizuki, N., & Asada, M. (2015). High-resolution magnetic signature of active hydrothermal systems in the back-arc spreading region of the southern Mariana trough. *Journal of Geophysical Research: Solid Earth*, *120*, 2821–2837. https://doi.org/10.1002/2014JB011714

Gemery-Hill, P. A., Shanks, W. C., Balistrieri, L. S., & Lee, G. K. (2007). Geochemical data for selected rivers, lake waters, hydrothermal vents, and subaerial geysers in Yellowstone National Park, Wyoming and vicinity, 1996–2004. In L. A. Morgan (Ed.), *Integrated geoscience studies in the greater Yellowstone area—Volcanic, tectonic, and hydrothermal processes in the Yellowstone geoecosystem*, *U.S. Geological Survey Professional Paper 1717* (pp. 365–426). Reston, VA: U.S. Geological Survey. Retrieved from https://pubs.usgs.gov/pp/1717/downloads/pdf/p1717L.pdf

Hochstein, M. P., & Soengkono, S. (1997). Magnetic anomalies associated with high temperature reservoirs in the Taupo volcanic zone (New Zealand). *Geothermics*, *26*(1), 1–24. https://doi.org/10.1016/S0375-6505(96)00028-4

Hunt, C. P., Moskowitz, B. M., & Banerjee, S. K. (1995). Magnetic properties of rocks and minerals. In *Rock physics & phase relations: A handbook of physical constants, AGU reference shelf* (Vol. 3, pp. 189–204). Washington DC: American Geophysical Union.

Husen, S., Smith, R. B., & Waite, G. P. (2004). Evidence for gas and magmatic sources beneath the Yellowstone volcanic field from seismic tomographic imaging. *Journal of Volcanology and Geothermal Research*, *131*(3–4), 397–410. https://doi.org/10.1016/S0377-0273(03)00416-5

Johnson, S. Y., Stephenson, W. J., Morgan, L. A., Shanks, W. C. III, & Pierce, K. L. (2003). Hydrothermal and tectonic activity in northern Yellowstone Lake, Wyoming. *Geological Society of America Bulletin*, *115*(8), 954–971. https://doi.org/10.1130/B25111.1

Knight, J.C. (1975). The limnology of the West Thumb of Yellowstone Lake, Yellowstone National Park, Wyoming (MSc thesis) (pp. 1–74). Montana State University.

Larson, P. B., Phillips, A., John, D., Cosca, M., Pritchard, C., Andersen, A., & Manion, J. (2009). A preliminary study of older hot spring alteration in Sevenmile Hole, Grand Canyon of the Yellowstone River, Yellowstone caldera, Wyoming. *Journal of Volcanology and Geothermal Research*, *188*(1–3), 225–236. https://doi.org/10.1016/j.jvolgeores.2009.07.017

Licciardi, J. M., & Pierce, K. L. (2008). Cosmogenic exposure-age chronologies of Pinedale and Bull Lake glaciations in Greater Yellowstone and the Teton Range, USA. *Quaternary Science Reviews*, *27*(7-8), 814–831. https://doi.org/10.1016/j.quascirev.2007.12.005

Licciardi, J. M., & Pierce, K. L. (2018). History and dynamics of the Greater Yellowstone glacial system during the last two glaciations. *Quaternary Science Reviews*, *200*, 1–33. https://doi.org/10.1016/j.quascirev.2018.08.027

Locke, W. W., Meyer, G. A., & Pings, J. C. (1992). Morphology of a postglacial fault scarp across the Yellowstone (Wyoming) caldera margin and its implications. *Bulletin of the Seismological Society of America*, *82*, 511–516.

Lowenstern, J. B., & Hurwitz, S. (2008). Monitoring a supervolcano in repose: Heat and volatile flux at the Yellowstone caldera. *Elements*, *4*, 35–40. https://doi.org/10.2113/GSELEMENTS.4.1.35

Matthews, N. E., Vazquez, J. A., & Calvert, A. T. (2015). Age of the Lava Creek supereruption and magma chamber assembly at Yellowstone based on $^{40}Ar/^{39}Ar$ and U-Pb dating of sanidine and zircon crystals. *Geochemistry, Geophysics, Geosystems*, *15*, 2508–2528. https://doi.org/10.1002/2015GC005881

Meyer, G. A., & Locke, W. W. (1986). Origin and deformation of Holocene shoreline terraces, Yellowstone Lake, Wyoming. *Geology*, *14*(8), 699–702. https://doi.org/10.1130/0091-7613(1986)14<699:OADOHS>2.0.CO;2

Morgan, L. A., & Shanks, W. C. (2005). Influences of rhyolitic lava flows on the hydrothermal processes in Yellowstone Lake and on the Yellowstone Plateau. In W. P. Inskeep, & T. R. McDermott (Eds.), *Geothermal Biology and Geochemistry in Yellowstone National Park* (pp. 31–52). Yellowstone National Park, Wyoming: Proceeding of the Thermal Biology Institute workshop.

Morgan, L. A., Shanks, W. C. III, Lovalvo, D. A., Johnson, S. Y., Stephenson, W. J., Pierce, K. L., et al. (2003). Exploration and discovery in Yellowstone Lake: Results from high-resolution sonar imaging, seismic reflection profiling, and submersible studies. *Journal of Volcanology and Geothermal Research*, *122*(3–4), 221–242. https://doi.org/10.1016/S0377-0273(02)00503-6

Morgan, L. A., Shanks, W. C. III, Pierce, K. L., Lovalvo, D. A., Lee, G. K., Webring, M. W., et al. (2007). The floor of Yellowstone Lake is anything but quiet—New discoveries from high-resolution sonar imaging, seismic-reflection profiling, and submersible studies. In L. A. Morgan (Ed.), *Integrated geoscience studies in the greater Yellowstone area, volcanic, hydrothermal, tectonic processes in the Yellowstone geoecosystem*, *U.S. Geological Survey Professional Paper 1717* (pp. 91–126). Reston, VA: U.S. Geological Survey. Retrieved from https://pubs.usgs.gov/pp/1717/downloads/pdf/p1717D.pdf

Morgan, L. A., Shanks, W. C. P., Lowenstern, J. B., Farrell, J. M., & Robinson, J. E. (2017). *Geologic field–trip guide to the volcanic and hydrothermal landscape of the Yellowstone Plateau. U.S. Geological Survey Scientific Investigations Report 2017–5022–P* (pp. 1–100). https://doi.org/10.3133/sir20175022P

Morgan, L. A., Shanks, W. C. P. III, & Pierce, K. L. (2009). Hydrothermal processes above the Yellowstone magma chamber: Large hydrothermal systems and large hydrothermal explosions. *Special Paper of the Geological Society of America*, *459*, 1–95. https://doi.org/10.1130/2009.2459

Morgan, P., Blackwell, D. D., Spafford, R. E., & Smith, R. B. (1977). Heat flow measurements in Yellowstone Lake and the thermal structure of the Yellowstone caldera. *Journal of Geophysical Research*, *82*(26), 3719–3732. https://doi.org/10.1029/JB082i026p03719

Morrell, A. E., Locke, C. A., Cassidy, J., & Mauk, J. L. (2011). Geophysical characteristics of adularia-sericite epithermal gold-silver deposits in the Waihi-Waitekauri region, New Zealand. *Economic Geology*, *106*(6), 1031–1041. https://doi.org/10.2113/econgeo.106.6.1031

Norton, D. R., & Friedman, I. (1985). Chloride flux out of Yellowstone National Park. *Journal of Volcanology and Geothermal Research*, *26*, 231–250. https://doi.org/10.1016/0377-0273(85)90058-7

Ohmoto, H. (2003). Non-redox transformations of magnetite-hematite in hydrothermal systems. *Economic Geology*, *98*, 157–161. https://doi.org/10.2113/gsecongeo.98.1.157

Otis, R. M., Smith, R. B., & Wold, R. J. (1977). Geophysical surveys of Yellowstone Lake, Wyoming. *Journal of Geophysical Research*, *82*(26), 3705–3717. https://doi.org/10.1029/JB082i026p03705

Pelton, J. R., & Smith, R. B. (1979). Recent crustal uplift in Yellowstone National Park. *Science*, *206*(4423), 1179–1182. https://doi.org/10.1126/science.206.4423.1179

Pelton, J. R., & Smith, R. B. (1982). Contemporary vertical surface displacements in Yellowstone National Park. *Journal of Geophysical Research*, *87*, 2,745–2,751. https://doi.org/10.1029/JB087iB04p02745

Phillips, J. D. (2007). Geosoft executables (GX's) developed by the U.S. Geological Survey, version 2.0, with notes on GX development from fortran code; OFR; 2007–1355

Pierce, K. L., Cannon, K. P., Meyer, G. A., Trebesch, M. J. & Watts, R. (2002). Post-glacial inflation–deflation cycles, tilting and faulting in the Yellowstone caldera based on Yellowstone Lake shorelines. *U.S. Geological Survey Open-File Report* 02–0142, 62 pp. https://doi.org/10.3133/ofr02142

Pierce, K. L., Cannon, K. P., Meyer, G. A., Trebesch, M. J., & Watts, R. D. (2007). Postglacial inflation-deflation cycles, tilting, and faulting in the Yellowstone caldera based on Yellowstone Lake shorelines. In L. A. Morgan (Ed.), *Integrated geoscience studies in the greater Yellowstone area, volcanic, hydrothermal, tectonic processes in the Yellowstone geoecosystem*, *U.S. Geological Survey Professional Paper 1717* (pp. 127–168). Reston, VA: U.S. Geological Survey. Retrieved from https://pubs.usgs.gov/pp/1717/downloads/pdf/p1717E.pdf

Prostka, H. J. (1973). Hybrid origin of the absarokite-shoshonite-banakite series, Absaroka volcanic field, Wyoming. *Geological Society of America Bulletin*, *84*, 697–702. https://doi.org/10.1130/0016-7606(1973)84<697:HOOTAS>2.0.CO;2

Reynolds, R. L. (1977). Paleomagnetism of welded tuffs of the Yellowstone group. *Journal of Geophysical Research*, *82*, 3677–3693. https://doi.org/10.1029/JB082i026p03677

Richmond, G. M. (1965). Glaciation of the Rocky Mountains. In H. E. Wright, Jr., & G. D. Frey (Eds.), *The Quaternary of the United States* (pp. 217–230). Princeton, N.J: Princeton University press.

Richmond, G. M. (1977). *Surficial geologic map of the Canyon Village quadrangle, Yellowstone National Park, Wyoming, U.S. Geological Survey, Map I–652, Scale 1:62,500*.

Shanks, W. C., Alt, J. C., & Morgan, L. A. (2007). Geochemistry of sublacustrine hydrothermal deposits in Yellowstone Lake—Hydrothermal reactions, stable-isotope systematics, sinter deposition, and spire growth. In L. A. Morgan (Ed.), *Integrated geoscience studies in the greater Yellowstone area, volcanic, hydrothermal, tectonic processes in the Yellowstone geoecosystem*, *U.S. Geological Survey Professional Paper 1717* (pp. 201–234). Reston, VA: U.S. Geological Survey. Retrieved from https://pubs.usgs.gov/pp/1717/downloads/pdf/p1717G.pdf

Shanks, W. C., Morgan, L. A., Balistrieri, L., & Alt, J. C. (2005). Hydrothermal vent fluids, siliceous hydrothermal deposits, and hydrothermally altered sediments in Yellowstone Lake. In W. P. Inskeep, & T. R. McDermott (Eds.), *Geothermal biology and geochemistry in Yellowstone National Park* (pp. 54–72). Yellowstone National Park, Wyoming: Proceeding of the Thermal Biology Institute workshop.

Shuey, R. T., Ugland, R. O., & Schmit, C. R. (1977). Magnetic properties and secular variation in cores from Yellowstone and Jackson Lakes, Wyoming. *Journal of Geophysical Research*, *82*(26), 3739–3746. https://doi.org/10.1029/JB082i026p03739

Smith, R. B., Jordan, M., Steinberger, B., Puskas, C. M., Farrell, J., Waite, G. P., et al. (2009). Geodynamics of the Yellowstone hotspot and mantle plume: Seismic and GPS imaging, kinematics, and mantle flow. *Journal of Volcanology and Geothermal Research*, *188*(1–3), 26–56. https://doi.org/10.1016/j.jvolgeores.2009.08.020

Sohn, R., Harris, R., Linder, C., Luttrell, K., Lovalvo, D., Morgan, L., et al. (2017). Exploring the restless floor of Yellowstone Lake. *Eos*, *98*. https://doi.org/10.1029/2017EO087035

Sohn, R. A., Luttrell, K., Shroyer, E., Stranne, C., Harris, R. N., & Favorito, J. E. (2019). Observations and modeling of a hydrothermal plume in Yellowstone Lake. *Geophysical Research Letters*, *46*, 6435–6442. https://doi.org/10.1029/2019GL082523

Studt, F. E. (1959). Magnetic survey of the Wairakei hydrothermal field. *New Zealand Journal of Geology and Geophysics*, *2*, 746–754. https://doi.org/10.1080/00288306.1959.10422768

Szitkar, F., & Dyment, J. (2015). Near-seafloor magnetics reveal tectonic rotation and deep structure at TAG (trans-Atlantic Geotraverse) hydrothermal site (mid-Atlantic Ridge, 26°N). *Geology*, *43*, 87–90. https://doi.org/10.1130/G36086.1

Szitkar, F., Dyment, J., Choi, Y., & Fouquet, Y. (2014). What causes low magnetization at basalt-hosted hydrothermal sites? Insights from inactive site Krasnov (MAR 16°38′N). *Geochemistry, Geophysics, Geosystems*, *15*, 1441–1451. https://doi.org/10.1002/2014GC005284

Tan, C., Cino, C. D., Ding, K., & Seyfried, W. E. (2017). High temperature hydrothermal vent fluids in Yellowstone Lake: Observations and insights from in-situ pH and redox measurements. *Journal of Volcanology and Geothermal Research*, *343*, 263–270. https://doi.org/10.1016/j.jvolgeores.2017.07.017

Tivey, M. A., & Dyment, J. (2010). The magnetic signature of hydrothermal systems in slow-spreading environments. In *Diversity of Hydrothermal Systems on Slow Spreading Ocean Ridges*, *Geophysical Monograph Series* (Vol. 188, pp. 43–66). Washington, D. C: American Geophysical Union. https://doi.org/10.1029/2008GM000773

Tivey, M. A., & Johnson, H. P. (2002). Crustal magnetization reveals subsurface structure of Juan de Fuca ridge hydrothermal vent fields. *Geology*, *30*, 979–982. https://doi.org/10.1130/0091-7613(2002)030<0979:CMRSSO>2.0.CO;2

Tivey, M. A., Johnson, H. P., Salmi, M. S., & Hutnak, M. (2014). High-resolution near-bottom vector magnetic anomalies over raven hydrothermal field, endeavour segment, Juan de Fuca ridge. *Journal of Geophysical Research: Solid Earth*, *119*, 7389–7403. https://doi.org/10.1002/2014JB011223

U.S. Geological Survey (2000). An aeromagnetic survey in Yellowstone National Park: A web site for distribution of data (on-line edition), *U.S. Geological Survey Open File Report* 00–163. http://pubs.usgs.gov/of/2000/ofr-00-0163/

White, D. E., Fournier, R. O., Muffler, L. J. P., & Truesdell, A. H. (1975). *Physical results of research drilling in thermal areas of Yellowstone National Park, Wyoming. U.S. Geological Survey Professional Paper 892* (pp. 1–70). https://doi.org/10.3133/pp892

White, D. E., Hutchinson, R. A., & Keith, T. E. (1988). *Geology and remarkable thermal activity of Norris Geyser Basin, Yellowstone National Park, Wyoming. U.S. Geological Survey Professional Paper 1456* Retrieved from https://pubs.usgs.gov/pp/1456/

White, D. E., Muffler, L. J. P., & Truesdell, A. H. (1971). Vapor-dominated hydrothermal systems compared with hot-water systems. *Economic Geology*, *66*, 75–97. https://doi.org/10.2113/gsecongeo.66.1.75

Wicks, C. W., Thatcher, W., Dzurisin, D., & Svarc, J. (2006). Uplift, thermal unrest and magma intrusion at Yellowstone caldera. *Nature*, *440*(7080), 72–75. https://doi.org/10.1038/nature04507

Wicks, C. W. Jr., Thatcher, W. R., & Dzurisin, D. (1998). Migration of fluids beneath Yellowstone caldera inferred from satellite radar interferometry. *Science*, *282*(5388), 458–462. https://doi.org/10.1126/science.282.5388.458

Wold, R. J., Mayhew, M. A., & Smith, R. B. (1977). Bathymetric and geophysical evidence for a hydrothermal explosion crater in Mary Bay, Yellowstone Lake, Wyoming. *Journal of Geophysical Research*, *82*(26), 3733–3738. https://doi.org/10.1029/JB082i026p03733

Wotzlaw, J.-F., Bindemen, I. A., Stern, R. A., D'Abzac, F. X., & Schaltegger, U. (2015). Rapid heterogenous assembly of multiple magma reservoirs prior to Yellowstone supereruptions. *Scientific Reports*, *5*, 14,026. https://doi.org/10.1038/srep14026

Zhao, J., Brugger, J., & Pring, A. (2018). Mechanism and kinetics of hydrothermal replacement of magnetite by hematite. *Geoscience Frontiers*, *10*(1), 29–41. https://doi.org/10.1016/j.gsf.2018.05.015

Zhu, J., Lin, J., Chen, Y. J., Tao, C., German, C. R., Yoerger, D. R., & Tivey, M. A. (2010). A reduced crustal magnetization zone near the first observed active hydrothermal vent field on the southwest Indian Ridge. *Geophysical Research Letters*, *37*, L18303. https://doi.org/10.1029/2010GL043542